Exploring possibilities for 2-butanol production in *A. woodii* by exchange of the ADH4 promoter

BACHELOR'S THESIS

submitted in partial fulfillment of the requirements for the degree of

Bachelor of Science

in

Technical Chemistry

by

Thomas Hackl
Registration Number 01526302

to the Research Group for Bioprocess Technology

at the TU Wien

Main advisor: Assistant Prof. Dipl.-Ing.(FH) Dr. Stefan Plügl
Co-advisor: Projektasse(FWF) Dipl.-Inge Klara Wögerbauer, BSc

Vienna, January 1, 2025

Thomas Hackl	Stefan Plügl

Declaration of Authorship

I hereby declare that I have written this Thesis independently, that I have completely specified the utilized sources and resources and that I have definitely marked all parts of the work - including tables, maps and figures - which belong to other works or to the internet, literally or extracted, by referencing the source as borrowed.

I further declare that I have used generative AI tools only as an aid, and that my own intellectual and creative efforts predominate in this work. In the appendix "Overview of Generative AI Tools Used" I have listed all generative AI tools that were used in the creation of this work, and indicated where in the work they were used. If whole passages of text were used without substantial changes, I have indicated the input (prompts) I formulated and the IT application used with its product name and version number/date.

Vienna, January 1, 2025

Thomas Hackl

Abstract

The aim of this bachelor's project was to enhance the microbial production of 2-butanol from 2,3-butanediol by modifying the expression of alcohol dehydrogenase 4 (ADH4) in *A. woodii*. To this end, the native promoter of adh4 was replaced with the stronger pta promoter from *Clostridium ljungdahlii* using a CRISPR/Cas9-based genome editing approach. Homology-directed repair with specific spacer sequences enabled targeted integration. Plasmid constructs were verified in *E. coli* and subsequently transformed into *A. woodii*. Correctly modified clones were confirmed via PCR and sequencing. The engineered strain was compared to the wild type under various substrate conditions, and product formation was analyzed by HPLC. However, no significant increase in 2-butanol production was observed, indicating that promoter replacement alone was insufficient to enhance the conversion of 2,3-butanediol to 2-butanol.

Contents

Abstract iii

Contents iv

1 Introduction 1
- 1.1 Acetobacterium woodii . . . 1
- 1.2 The Wood-Ljungdahl pathway . . . 2
- 1.3 2-Butanol metabolism . . . 2
- 1.4 CRISPR-based genome editing . . . 3
- 1.5 Golden Gate Cloning . . . 4
- 1.6 Aim of the work . . . 5

2 Materials and methods 6
- 2.1 Preparation of Serum Bottles for Anaerobic Cultivation Experiments . . . 6
- 2.2 Preparation of Agar Plates . . . 6
- 2.3 Pre-cultivation of *A. woodii* Strains TU2.0 and Δaco1 . . . 7
- 2.4 Preparation of HPLC Standards . . . 8
- 2.5 Molecular Biology Methods . . . 8
- 2.6 Serum Bottle Experiments for 2-butanol Production Analysis . . . 9
- 2.7 Sampling and HPLC Sample Preparation . . . 10
- 2.8 Determination of 2-butanone and 1-propanol by Overlapping RI Peak Analysis . . . 11
- 2.9 Methodology for Carbon Balance Determination . . . 12

3 Results and Evaluation 14
- 3.1 Construction of the CRISPR array plasmid . . . 14
- 3.2 Transformation of the CRISPR array plasmid into *A. woodii* . . . 15
- 3.3 Serum Bottle Experiments for 2-butanol Production Analysis . . . 16

4 Discussion 26
- 4.1 Promoter Exchange of ADH4 in *A. woodii* . . . 26
- 4.2 Effect of 1,2-Propanediol on 2-Butanol Formation . . . 26
- 4.3 Carbon balance of mixed-substrate fermentations . . . 27
- 4.4 Hypothesis on the Preferential Use of the Wood-Ljungdahl Pathway under H_2 Conditions 27
- 4.5 Challenges in HPLC quantification of 2-butanol . . . 27
- 4.6 Outliers in Optical Density Measurements . . . 28

5 Outlook 29

List of Figures 30

List of Tables 33

Bibliography 34

Anhang A: HPLC Standards 37

Appendix B: Primer 38

CHAPTER 1

Introduction

The increasing demand for sustainable chemicals has highlighted the need for efficient microbial production of bio-based alcohols. 2-Butanol is an important platform chemical with applications as a fuel additive and in the chemical industry. *Acetobacterium woodii*, an acetogenic bacterium, is capable of producing various alcohols via the Wood-Ljungdahl pathway, making it a promising host for biotechnological production [BSTW77, Lju86, Woo91].

Alcohol dehydrogenases (ADHs) catalyze the reduction of ketones to alcohols and play a key role in 2-butanol biosynthesis. In *A. woodii*, ADH4 has been identified as a potential bottleneck for 2-butanol formation. Enhancing its expression through promoter engineering could increase product yield.

In wild-type *A. woodii*, 2,3-butanediol is partially oxidized to acetoin, which is then converted into 2-acetyl-CoA by the enzyme acetoin:CoA transferase (Aco1) and subsequently yields acetate [Fuc86, Die92]. To redirect carbon flux toward 2-butanol, a knockout of the *aco1* gene (Δaco1) was implemented. This modification blocks the conversion of acetoin to 2-acetyl-CoA, thereby increasing the likelihood that the carbon from 2,3-butanediol is channeled into 2-butanone (MEK) and subsequently reduced to 2-butanol [DSD$^+$87, Dra94].

The objective of this study was therefore twofold: first, to investigate the effect of promoter strength on 2-butanol production by replacing the native ADH4 promoter with stronger alternatives, and second, to compare the metabolic performance of wild-type and Δaco1 strains under different substrates and gas atmospheres.

1.1 Acetobacterium woodii

Acetobacterium woodii is a strictly anaerobic, gram-positive acetogen first isolated from marine sediments [BSTW77]. It utilizes the Wood-Ljungdahl pathway as its central metabolic route, enabling growth on H_2 and CO_2 as sole energy and carbon sources [Lju86, Woo91]. In addition to autotrophic growth, it can ferment a wide range of organic substrates such as fructose or lactate.

Widely present in anoxic ecological niches, including bottom sediments of seas and freshwater bodies, methanogenic communities, or hot springs, acetogens like *A. woodii* annually fix significant amounts of CO2 [Deb21]. The acetogenic metabolism is considered ancient, with the Wood-Ljungdahl pathway likely existing for up to 4 billion years [Mar20].

Due to its robust anaerobic metabolism and well-characterized physiology, *A. woodii* has become a model organism for studying acetogenesis. It is considered non-pathogenic and safe to handle under laboratory conditions [Die92]. Classical studies have demonstrated its metabolic flexibility, including the ability to produce ethanol and other alcohols under specific conditions, which makes it a promising candidate for biotechnological applications [DSD$^+$87, Dra94].

Furthermore, *A. woodii* is genetically accessible, with established tools for targeted mutagenesis and promoter engineering, facilitating diverse metabolic engineering approaches. [Dra94].

1.2 The Wood-Ljungdahl pathway

The Wood-Ljungdahl pathway (WLP), also known as the reductive acetyl-CoA pathway, is the central carbon fixation route in acetogenic bacteria such as *A. woodii*. It enables the conversion of CO_2 into acetyl-CoA, which serves as both a precursor for biomass formation and as a substrate for the synthesis of various metabolites [Lju86, Woo91, Fuc86], as illustrated in Figure 1.1

The pathway is divided into two branches: (i) the methyl branch, where CO_2 is sequentially reduced to formate and further converted to a methyl group bound to tetrahydrofolate, and (ii) the carbonyl branch, in which CO_2 is reduced to carbon monoxide by carbon monoxide dehydrogenase. Both branches converge at the acetyl-CoA synthase complex, which combines the methyl group, carbon monoxide, and coenzyme A to form acetyl-CoA [Rag91].

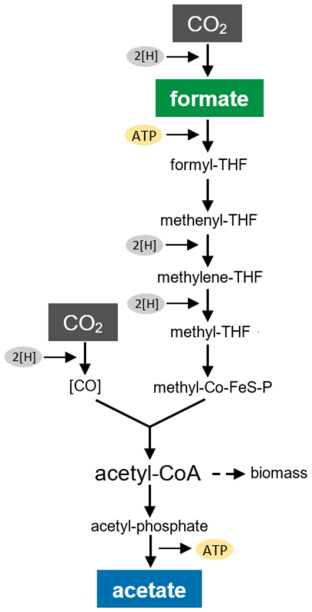


Figure 1.1: Schematic representation of the Wood–Ljungdahl pathway (WLP) in *A. woodii*, showing the methyl and carbonyl branches that come together in the formation of acetyl-CoA. Adapted from Klara Wögerbauer.

In *A. woodii*, the WLP not only supports autotrophic growth on CO_2 and H_2, but also plays a key role in energy conservation via electron bifurcation and sodium ion gradients, making it a highly efficient system for anaerobic metabolism [Die92, Dra94].

1.3 2-Butanol metabolism

In *A. woodii*, the formation of 2-butanol is linked to the metabolism of 2,3-butanediol (2,3-BD). The diol is oxidized by the diol dehydratase complex PduCDE to 2-butanone (MEK), which catalyzes this reaction in acetogenic bacteria [OSS91]. The subsequent reduction of 2-butanone to 2-butanol is catalyzed by the alcohol dehydrogenase PduQ (ADH4) using NADH. However, ADH4 exhibits only low activity toward 2-butanone, leading to accumulation of the intermediate and a limited production of 2-butanol [SSL+15]. This enzymatic bottleneck represents a major limitation for 2-butanol production in acetogens.

The enzyme PduQ belongs to the family of iron-dependent alcohol dehydrogenases (group III) and is evolutionarily specialized in the conversion of short-chain alcohols and aldehydes. Its characteristic

function is the NAD^+-dependent oxidation of alcohols to aldehydes or, conversely, the NADH-dependent reduction of aldehydes to alcohols. Its physiological role was originally characterized in the context of 1,2-propanediol degradation in *Salmonella enterica*, where it is an integral component of a bacterial microcompartment (MCP) and essential for maintaining efficient metabolic flux through internal regeneration of NAD^+ from NADH [CFSB12]. The low activity of *A. woodii* PduQ toward the non-physiological substrate 2-butanone highlights its specific adaptation to its natural substrate range in 1,2-propanediol metabolism.

In parallel, 2,3-BD can be converted to acetoin via budC ($NAD^+ \rightarrow$ NADH) [HOTM15]. Acetoin is subsequently metabolized by the Aco enzyme complex to acetaldehyde and acetyl-CoA (also $NAD^+ \rightarrow$ NADH) [OSS91, HOTM15]. Acetaldehyde can be further oxidized to acetyl-CoA, part of which is converted to acetate, thereby generating ATP [HOTM15].

The overall pathway is shown in Figure 1.2.

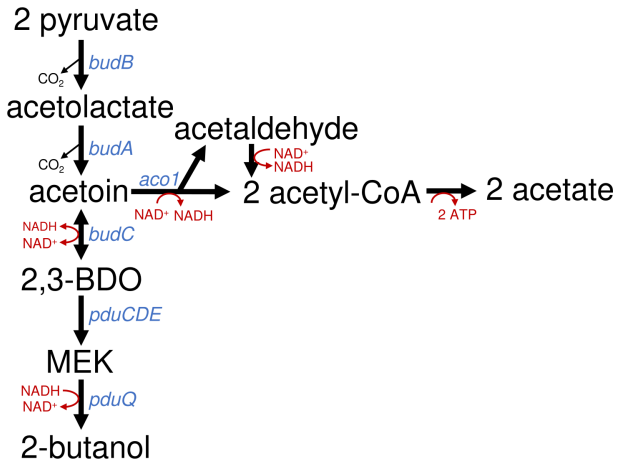


Figure 1.2: Schematic representation of the 2,3-butanediol metabolism in *A. woodii*. 2,3-butanediol is oxidized by the PduCDE complex to 2-butanone (MEK), which can be reduced to 2-butanol by PduQ (ADH4). Simultaneously, 2,3-butanediol can be converted to acetoin by budC, which is then transformed to acetaldehyde and two molecules of acetyl-CoA via Aco1. Acetaldehyde can be further oxidized to acetyl-CoA, with one acetyl-CoA molecule converted to acetate with concomitant ATP formation. Adapted from Klara Wögerbauer.

1.4 CRISPR-based genome editing

For genetic modifications in *A woodii*, the endogenous Type I-B CRISPR/Cas system offers an effective alternative to heterologous CRISPR-Cas9 systems, which are difficult to use in this organism because of nuclease toxicity and restriction barriers [PDBM+23]. In this study, this native system was applied for promoter replacement.

The approach uses an editing vector that carries a synthetic CRISPR array and a donor DNA template for homologous recombination. The synthetic array mimics the native arrays of *A. woodii*; it is controlled by the native leader sequence [ZHA+13, MKKK19, PDBM+23] and contains a spacer (targeting the genomic locus of interest) flanked by direct repeats (DRs). Once expressed, the array is processed into crRNA, which guides the Cascade effector complex to the DNA target next to a protospacer adjacent motif (PAM). In Type I-B systems, PAMs often contain double cytosines [BSM+15, MKB+19]. In *A. woodii*, the functional PAM was identified as 5´-CCA-3´ [PDBM+23]. After Cascade binding, the Cas3 nuclease is recruited and introduces a double-strand break near the target site [MB13, SJD+11, WvDB+11].

For promoter replacement, the donor template contained either the *pta* promoter from *C. ljungdahlii* or the *rso5* promoter from *A. woodii*, flanked by left and right homology arms (LHA and RHA) matching the sequences next to the Cas3 cleavage site. This design promotes homologous recombination

[PDBM+23], which allows the native promoter to be replaced by the new one. Cells that undergo this recombination also avoid further cleavage by the CRISPR machinery, which facilitates their selection. In this way, the cell's own defense system is used for genome engineering while avoiding the toxicity linked to heterologous Cas9 expression [PDBM+23].

The overall workflow of this mechanism is illustrated in Figure 1.3.

Using the endogenous CRISPR system for knock-in strategies such as promoter exchange demonstrates its potential for advanced metabolic engineering in the otherwise hard-to-edit acetogen *A. woodii* [PDBM+23].

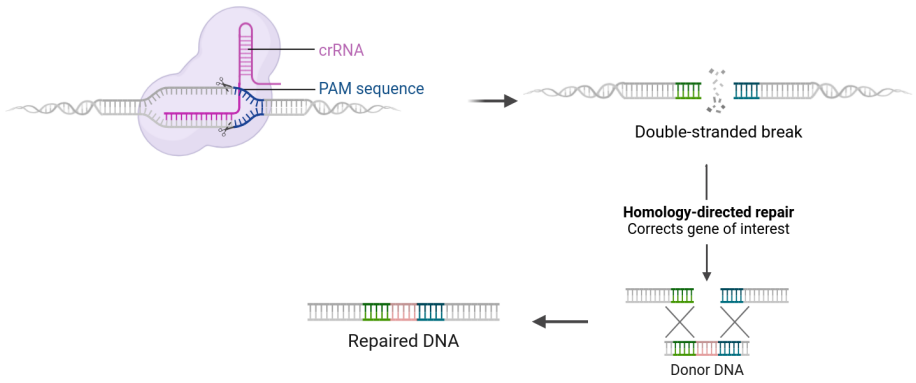


Figure 1.3: Schematic overview of the endogenous Type I-B CRISPR/Cas system mediated promoter replacement in *A. woodii*. A synthetic CRISPR array provides a crRNA that guides the Cascade complex to the target site next to a PAM sequence. Cas3 is then recruited and introduces a double-strand break in the genomic DNA. Homologous recombination with a donor DNA template containing the new promoter flanked by left and right homology arms (LHA and RHA) enables the integration of the modified sequence. (Adapted from a BioRender template by Esmée Dragt (biorender.com).)

This application of the endogenous CRISPR system for a knock-in strategy, such as promoter exchange, demonstrates its utility for advanced metabolic engineering in the genetically recalcitrant acetogen *A. woodii* [PDBM+23].

1.5 Golden Gate Cloning

Golden Gate cloning is a versatile and efficient DNA assembly method that utilizes type IIS restriction enzymes, such as *BsaI* or *BpiI*, in combination with T4 DNA ligase [EKM08, WEG+11]. Unlike conventional restriction enzymes, type IIS enzymes cut outside of their recognition site, generating user-defined overhangs that enable the seamless assembly of multiple DNA fragments in a predefined order, as illustrated in Figure 1.4.

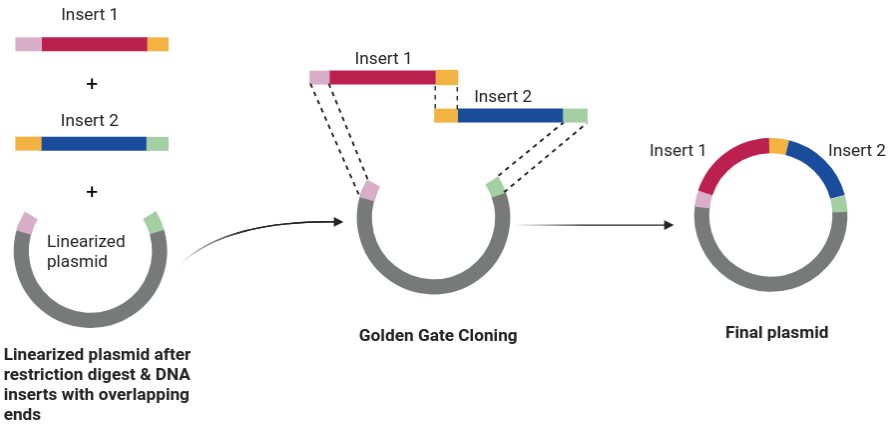


Figure 1.4: Schematic overview of the Golden Gate cloning process. (1) Linearized plasmid and DNA inserts with designed overhangs. (2) Complementary overhangs anneal. (3) T4 DNA ligase seals the nicks, yielding the final assembled plasmid. (Adapted from a BioRender template by Samara Ona (biorender.com).)

The method is performed in a single-pot reaction, where digestion and ligation occur simultaneously in a thermocycling program. This enables high efficiency and fidelity, as correctly ligated products no longer contain recognition sites for the restriction enzyme and are therefore protected from further cleavage [EKM08].

Due to its modularity and efficiency, Golden Gate cloning has become widely used in synthetic biology and metabolic engineering for the rapid construction of plasmids, promoter libraries, and entire operons [EYG+14, POM+15]. In this study, the method was applied to construct a donor template for the endogenous Type I-B CRISPR/Cas system in *A. woodii*. The template contained left and right homology arms (LHA and RHA) flanking the new promoter sequence, enabling precise replacement of the native *adh4* promoter with stronger variants. Additionally, the template carried the synthetic CRISPR array, which produces crRNAs guiding the native Cascade complex and Cas3 nuclease to the correct genomic target site for DNA cleavage and homologous recombination.

1.6 Aim of the work

The aim of this work was to investigate strategies for improving 2-butanol production in *A. woodii*. Specifically, the objectives were:

- Increase the expression of *adh4* by replacing its native promoter with a stronger one.
- Test whether 2-butanol is produced when 2,3-butanediol and another diol are provided as co-substrates.
- Evaluate the effect of molecular hydrogen on the cellular redox balance and its potential to enhance 2-butanol formation.

CHAPTER 2

Materials and methods

2.1 Preparation of Serum Bottles for Anaerobic Cultivation Experiments

Table 2.1: Ingredients for 1 L of the defined growth medium

Component	Amount
10x phosphate A	100 mL
10x salt A	100 mL
$NaHCO_3$	10 g
TE stock (1000x)	4 mL
Fe stock	0.074 mL
Resazurin stock	0.5 mL



The ingredients listed in Table 2.1 correspond to 1 L of medium. For the preparation of 0.5 L, all components were proportionally scaled down by half.

For the serum bottle experiments, 0.5 L of the defined medium was prepared by transferring 50 mL of 10× phosphate A and 50 mL of 10× salt A into a 0.5 L laboratory flask using a 50 mL flask. The mixture was then supplemented with 5 g $NaHCO_3$, as well as 18 µL Fe stock solution and 0.25 mL resazurin stock solution, which caused the solution to darken almost to black.



After filling the laboratory flask up to 0.5 L with deionized water, the color appeared as a rich blue.

The flask was then degassed with an N_2/CO_2 gas mixture (flow rate: 0.5 L/min) in an 80:20 ratio. After a slight violet coloration, 0.25 g cysteine-HCl·H_2O was added, and degassing was continued until the medium took on a light pink color.

The serum bottles were then degassed for approximately 3 minutes. Using a dispensing device, 20 mL of the medium was added to each bottle, followed by an additional 3 minutes of degassing until the liquid exhibited only a faint pink hue. The bottles were then sealed with rubber stoppers, secured by crimped aluminum caps.

The solution completely lost its color after final autoclaving of the bottles.

2.2 Preparation of Agar Plates

The ingredients listed in Table 2.2 correspond to 1 L of medium. For the preparation of 0.5 L, all components were proportionally scaled down by half.

Table 2.2: Composition of 1 L undefined medium for agar plates.

Component	Amount
10× Phosphate B	100 mL
10× Salt B	100 mL
Yeast Extract	1 g
$NaHCO_3$	3 g
TE 1000×	2 mL
Fe Stock	0.074 mL
Resazurin Stock	0.5 mL
Agar	15 g

To prepare agar plates, 0.5 L of the undefined medium was prepared. For this purpose, 50 mL of 10× phosphate B and 50 mL of 10× salt B were transferred into a laboratory bottle. Subsequently, 0.5 g of yeast extract and 1.5 g of sodium carbonate were weighed and added to the bottle. Then, 1 mL of 1000× TE buffer, 37 µL of Fe stock solution, and 0.25 mL of resazurin stock were pipetted in, causing the solution to turn nearly black. Finally, 7.5 g of agar was weighed, added to the bottle, and the volume was adjusted to 0.5 L with deionized water, which resulted in an intense blue coloration of the medium.

The bottle was autoclaved and subsequently cooled down to a temperature suitable for the addition of the appropriate antibiotic for the bacterial strain (see Table 2.3). The medium was then dispensed into petri dishes within the laminar flow hood so that the bottom was just covered with liquid.

Table 2.3: Antibiotics used for the bacterial strains

Bacterial Strain	Strain ID	Antibiotic
Escherichia coli	SPF 2042	Carbenicillin
Escherichia coli	SPF 3051	Chloramphenicol
Acetobacterium woodii	—	Thiamphenicol

2.3 Pre-cultivation of *A. woodii* Strains TU2.0 and Δaco1

Table 2.4: Composition of 1 L undefined medium

Component	Amount
10× phosphate A	100 mL
10× salt A	100 mL
Yeast extract	2 g
Sodium bicarbonate ($NaHCO_3$)	10 g
TE 1000×	2 mL
Fe stock solution	0.037 mL
Resazurin stock solution	0.5 mL

The ingredients listed in Table 2.4 correspond to 1 L of medium. For the preparation of 0.5 L, all components were proportionally scaled down by half.

For the preparation of 0.5 L of undefined growth medium, 50 mL of 10× phosphate A and 50 mL of 10× salt A were transferred into a laboratory bottle. Subsequently, 1 g of yeast extract and 5 g of sodium carbonate were weighed and added to the bottle, along with 18.5 µL of Fe stock solution and 0.25 mL of resazurin stock solution, which caused the solution to turn nearly black. Upon filling the bottle up to 0.5 L with deionized water, the medium assumed a deep blue color.

Degassing of the medium and preparation of the serum bottles were performed analogously as described in Section 2.1.

Finally, 1 mL of a prepared cell culture of each respective strain was injected into separate serum bottles using a sterile syringe—one bottle containing *A. woodii* strain TU2.0, and the other containing strain Δaco1. The cultures were then incubated in a shaking incubator at 30 °C and 100 rpm.

2.4 Preparation of HPLC Standards

HPLC (High-performance liquid chromatography) standards were prepared gravimetrically, without using stock solutions. For each target concentration, the required amount of pure compound was calculated using the molar mass, the desired concentration, and the target volume, according to equation 2.1. When necessary, the purity of the compound was also taken into account. The calculated amount of each standard was weighed using an analytical balance, dissolved in deionized water, and brought to a final volume using a volumetric flask (typically 10–25 mL, chosen to facilitate convenient handling and accurate weighing).

$$m = c \cdot V \cdot \frac{M}{P} \tag{2.1}$$

where:
m = required mass of the substance [g]
c = target concentration of the solution [mol/L or g/L]
V = final volume of the solution [L]
M = molar mass of the substance [g/mol]
P = purity of the substance (e.g., 0.98 for 98% purity)

All calibration standards prepared for this study are listed in the Appendix (Table 1).

2.5 Molecular Biology Methods

2.5.1 Construction of the CRISPR array plasmid

In the first step of constructing the CRISPR array, the primers KWO_113 and KWO_125 (for spacer gRNA 2), as well as KWO_113 and KWO_127 (for spacer gRNA 1), were annealed using a temperature program over 10 minutes.

In the meantime, the homologous regions (LHA and RHA) and the RSO5 promoter were amplified by PCR from the *A. woodii* genome, and the pta promoter from the *Clostridium ljungdahlii* genome, using the B7 High Fidelity DNA Polymerase (Biozym Scientific GmbH, Hessisch Oldendorf, Germany) according to the manufacturer's protocol.

To verify the PCR products, agarose gel electrophoresis was performed. For gel preparation, 4 g of agarose were dissolved in 50 mL of 1× TAE (TRIS-Acetat-EDTA) buffer by heating the mixture in a microwave until the agarose was fully melted (approximately 1 minute), and subsequently stained with 3 µL of SYBR™ Safe DNA Gel Stain (Thermo Fisher Scientific, Waltham, MA, USA). After casting the gel, the PCR products were loaded alongside a 1 kb Plus DNA ladder (Thermo Scientific™ GeneRuler) and run at 100 V for approximately 45 minutes.

Next, the two spacers were cloned into separate plasmids (spf-2042) using Golden Gate assembly and subsequently transformed into *E. coli* by heat shock. Selection was performed on LB agar plates supplemented with carbenicillin, as the plasmid backbone carries an carbenicillin resistance gene.

The overnight-grown cells were screened for the presence of the spacer by colony PCR using the YourTaq™ Direct-Load PCR Master Mix (biotechrabbit GmbH, Berlin, Germany), followed by gel electrophoresis. The correct assembly and completeness of the plasmid were validated through Sanger

sequencing. Positive clones were used to inoculate 3 mL overnight cultures in culture tubes containing LB medium supplemented with carbenicillin, and the plasmid DNA was isolated using the HiYield Plasmid Mini Kit (SLG GmbH, Germany), following the manufacturer's protocol.

In the second step of constructing the CRISPR array, the DNA fragments for LHA, RHA, the promoters, and the spacer region (cloned into the spf-2042 plasmid) were assembled into the *E. coli* spf-3051 plasmid using Golden Gate assembly. Two separate plasmids were constructed: one containing the pta promoter and the other containing the RSO5 promoter. These plasmids were subsequently transformed into *E. coli* via heat shock. Selection was performed on LB agar plates supplemented with chloramphenicol, as the plasmid backbone (spf-3051) confers resistance to chloramphenicol. Overnight-grown clones were screened by colony PCR (biotechrabbit YourTaq™ Direct-Load PCR Master Mix) and gel electrophoresis for the presence of the homologous regions and promoters. Additionally, the constructs were verified by Sanger sequencing.

After confirming the completeness of the plasmid, an overnight culture was started in a 250 mL Erlenmeyer flask containing 50 mL of LB medium supplemented with chloramphenicol, and the plasmid DNA was isolated using the NucleoBond® Xtra Midi kit (Macherey-Nagel GmbH & Co. KG, Düren, Germany), following the manufacturer's instructions.

2.5.2 Transformation of the CRISPR array plasmid into *A. woodii*

Transformation of *A. woodii* was performed via electroporation under strictly anaerobic conditions according to an internal protocol (K. Wögerbauer, *Acetobacterium woodii* transformation, 2024). Cells were grown overnight to an OD_{600} of approximately 0.35 in fructose- and vitamin-supplemented medium. After harvesting by centrifugation, the cells were washed with ice-cold SMP buffer and concentrated to a final volume of 200 µL per transformation.

Electroporation was carried out using 200 µL of competent cells and approximately 10 µL of plasmid DNA in a 1 mm cuvette with the following parameters: 1.0 kV, 200 Ω, 50 µF (time constant ~6-9 ms). Immediately after the electric pulse, 1 mL of recovery medium was added, and the mixture was transferred into a Hungate tube containing 9 mL pre-reduced AWO_0007_BMY medium. Tubes were flushed with N_2/CO_2 and incubated anaerobically at 30 °C for 6 h.

After transformation, cells were plated on selective agar medium supplemented with cysteine and thiamphenicol, with TU and Δaco1 transformations on separate plates. All plates were incubated together in an anaerobic box (GasPak system) until colonies appeared, requiring up to 12 days. From each plate, a single colony was picked and consecutively numbered (colonies 1–6 for TU2.0, colonies 7–12 for Δaco1) and inoculated into selective-free li[illegible] medium in well plates. After 2 days of cultivation, lysates were prepared by heat treatment at 200 °C, and colony PCR was performed using B7 High Fidelity DNA Polymerase with primers KWO_139 and KWO_137 to screen for colonies showing the expected 1600 bp band.

2.6 Serum Bottle Experiments for 2-butanol Production Analysis

20 mL of defined medium (CDM) were dispensed into serum bottles and, under anaerobic conditions, supplemented by syringe injection with 0.4 mL of a vitamin solution, 2,3-butanediol as the main carbon source, and either propanediol, ethylene glycol, or methanol as cosubstrates. 1 mL Precultures of the strains TU2.0 or Δaco1 were inoculated into the bottles (see Table 2.5).

The TU2.0 strain served as the wild-type control expressing adh4 under its native promoter. The Δaco1 strain is a knockout mutant in which the aco1 gene, encoding acetoin:CoA transferase, is disrupted. This modification is intended to block the conversion of acetoin to 2-acetyl-CoA, potentially redirecting carbon flux toward 2-butanone and 2-butanol formation.

Table 2.5: Codes and details for serum bottles with strains expressing native promoter (strain and carbon source).

Code	Strain	C-source
A – C	TU2.0	2,3-butanediol (20 mM)
D – F	TU2.0	2,3-butanediol (20 mM) + methanol (50 mM)
G – I	Δaco1	2,3-butanediol (20 mM)
J – L	Δaco1	2,3-butanediol (20 mM) + methanol (50 mM)
M – N	TU2.0	2,3-butanediol (20 mM) + 1,2-propanediol (15 mM)
O – P	TU2.0	2,3-butanediol (20 mM) + ethylene glycol (20 mM)
Q – R	Δaco1	2,3-butanediol (20 mM) + 1,2-propanediol (15 mM)
S – T	Δaco1	2,3-butanediol (20 mM) + ethylene glycol (20 mM)

For the transformed *A. woodii* strains, the preparation of serum bottles was carried out analogously; however, the experimental setup was modified. While triplicate samples remained the same, the duplicate samples were incubated under a hydrogen atmosphere instead of nitrogen (see Table 2.6).

Table 2.6: Codes and details for serum bottles with transformed *A. woodii* strains expressing the *pta* promoter (strain and carbon source).

Code	Strain	C-source
pA – pC	TU2.0_Ppta	2,3-butanediol (20 mM)
pD – pF	TU2.0_Ppta	2,3-butanediol (20 mM) + methanol (50 mM)
pG – pI	Δaco1_Ppta	2,3-butanediol (20 mM)
pJ – pL	Δaco1_Ppta	2,3-butanediol (20 mM) + methanol (50 mM)
H1 – H2	TU2.0_Ppta	2,3-butanediol (20 mM)
H3 – H4	TU2.0_Ppta	2,3-butanediol (20 mM) + methanol (50 mM)
H5 – H6	TU2.0_Ppta	2-butanone (20 mM) + 1,2-propanediol (15 mM)

2.7 Sampling and HPLC Sample Preparation

To monitor cell growth and anaerobic conditions, optical density was measured at 600 nm (OD_{600}) and 660 nm (OD_{660}) using a ONDA V-10 Plus UV/VIS spectrophotometer (ONDA, Milan, Italy), respectively. For this purpose, 1 mL of culture was withdrawn directly from the serum bottle using a sterile syringe. After OD measurement, the same sample was used for HPLC preparation.

For HPLC analysis, the 1 mL sample was centrifuged at 21,000 × g for 10 minutes. The supernatant was transferred to a fresh tube, and the cell pellet was discarded. Subsequently, 540 µL of the supernatant were mixed with 60 µL of 40 mM sulfuric acid, vortexed thoroughly, and centrifuged again at 21,000 × g for 10 minutes. A volume of 540 µL of the clarified sample was transferred into an HPLC vial for analysis.

HPLC analysis was performed using a Vanquish Core HPLC system equipped with a Vanquish Variable Wavelength Detector F and a Refractomax520 detector (Thermo Fisher Scientific, Wilmington, United States). Separation was carried out on an Aminex HPX-87H column (Bio-Rad, Hercules, United States). The mobile phase consisted of 4 mM sulfuric acid (H_2SO_4) at a flow rate of 0.6 mL/min. A sample volume of 10 µL was injected, and each run lasted 45 minutes. Detection was performed

primarily using a refractive index (RI) detector, with additional UV detection at 280 nm. Data analysis was conducted using Chromeleon CDS software (Thermo Fisher Scientific, Wilmington, United States).

Further data analysis and visualization were performed using Python (version 3.12.3) with the libraries openpyxl, pandas, NumPy, SciPy, and Matplotlib.

2.8 Determination of 2-butanone and 1-propanol by Overlapping RI Peak Analysis

The peak of 1-propanol overlaps with the peak of 2-butanone in the refractive index (RI) spectrum due to identical retention times, which complicates the quantification of both 2-butanone and 1-propanol. Therefore, butanone was quantified based on its UV280 absorption spectrum.

Figure 2.1 shows the calibration curve for 2-butanone, created from the RI data by performing linear regression of the measured concentrations and their corresponding peak areas.

Equation (2.2) was used to convert the butanone concentration determined from the UV280 measurement into an equivalent RI peak area.

$$A_{\mathrm{MEK}} = 0.0975 \cdot C_{\mathrm{MEK}}^{\mathrm{UV}} - 0.0371 \tag{2.2}$$

where:
A_{MEK} = Peak area of 2-butanone in RI spectrum
$C_{\mathrm{MEK}}^{\mathrm{UV}}$ = Concentration of 2-butanone measured by UV280

Equation (2.3) was used to calculate the concentration of 1-propanol by subtracting the calculated butanone peak area from the total peak area (2-butanone + 1-propanol) to isolate the peak area corresponding to 1-propanol.

$$A_{\mathrm{C3}} = A_{\mathrm{total}} - A_{\mathrm{MEK}} \tag{2.3}$$

where:
A_{C3} = Peak area of 1-propanol in RI spectrum
A_{total} = Total peak area of 1-propanol and 2-butanone in RI spectrum
A_{MEK} = Peak area of 2-butanone in RI spectrum

Finally, the remaining RI peak area was converted back into a 1-propanol concentration using the calibration curve obtained from a 1-propanol standard (Equation (2.4), Figure 2.2).

$$C_{\mathrm{C3}} = \frac{A_{\mathrm{C3}} + 0.0178}{0.0812} \tag{2.4}$$

where:
C_{C3} = Concentration of 1-propanol
A_{C3} = Peak area of 1-propanol in RI spectrum

This approach allows the separation of overlapping peaks in the RI spectrum and enables accurate quantification of both compounds.

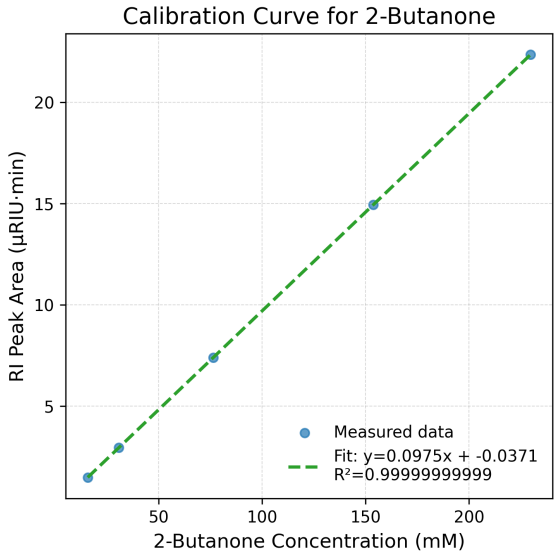


Figure 2.1: Linear regression of refractive index (RI) peak areas against known 2-butanone concentrations. The resulting calibration equation allows conversion of concentrations determined from UV280 spectra into expected RI peak areas.

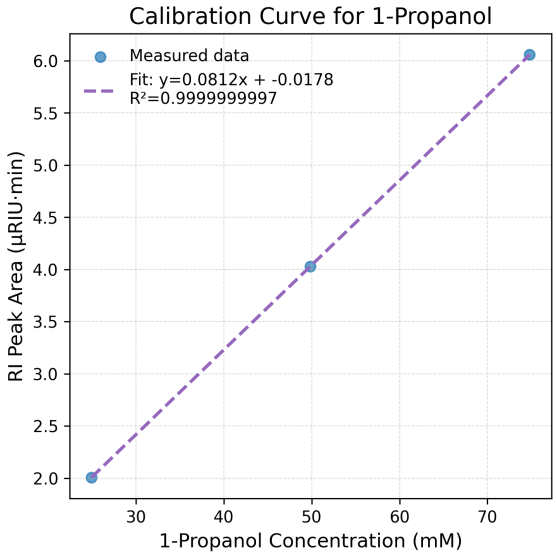


Figure 2.2: Linear regression of the calibration curve for 1-propanol, relating RI peak areas to known concentrations. The resulting regression equation enables conversion of calculated peak areas into concentrations.

2.9 Methodology for Carbon Balance Determination

To evaluate the distribution of carbon during fermentation, a carbon mass balance was performed. The carbon content of each detected soluble product was calculated by multiplying its molar concentration with the respective number of carbon atoms per molecule (see Table 2.7). The total amount of carbon recovered in the fermentation products and biomass was then compared to the initial amount of carbon introduced with the substrate. For comparative purposes, the total input carbon was normalized to 1, allowing for a relative assessment of carbon recovery across different experimental conditions.

Table 2.7: Overview of relevant compounds used for carbon balancing. The number of carbon atoms per molecule was used to calculate mmol of carbon from measured concentrations.

Compound	Molecular Formula	C Atoms / Molecule
2,3-Butanediol	$C_4H_{10}O_2$	4
Acetate	$C_2H_4O_2$	2
2-Butanone	C_4H_8O	4
Propionate	$C_3H_6O_2$	3
1-Propanol	C_3H_8O	3
Ethylene glycol	$C_2H_6O_2$	2
Methanol	CH_4O	1
Ethanol	C_2H_6O	2
1,2-Propanediol	$C_3H_8O_2$	3
Biomass	–	–
Propionaldehyde	C_3H_6O	3

To estimate the carbon content of the biomass, the optical density at 600 nm (OD600) measured in Section 2.7 was used. For *A. woodii*, an empirical conversion factor of 0.38 g/L (cell dry weight, CDW) per unit of OD600 was applied [NVD+21], as shown in Equation 2.5.

$$CDW = OD600 \cdot 0.38 \, \frac{g}{L} \tag{2.5}$$

The carbon mass in the biomass was subsequently calculated assuming a carbon content of 45% (w/w) of the dry weight [GLR90], using Equation 2.6. In this calculation, a molecular weight of 12 g/mol was used for carbon, and a conversion factor of 1000 was applied to convert from g/L to mmol/L. This approximation allows a rough estimation of the biogenic carbon distribution in the system.

$$\mathrm{C_{biomass}} = \mathrm{CDW} \cdot 0.45 \cdot \frac{1}{12} \cdot 1000 \tag{2.6}$$

For the soluble fermentation products, the expected conversion pathways were assumed (see Table 2.8). The resulting balance allowed an estimation of how much of the carbon introduced with the substrate could be recovered in the measured products.

Table 2.8: Assumed carbon flow from substrate compounds to observed products for carbon balancing.

Substrate	**Observed / Assumed Products**
2,3-Butanediol	2,3-Butanediol, 2-Butanone, 2-Butanol, Acetate
Methanol	Methanol, Acetate
1,2-Propanediol	1,2-Propanediol, 1-Propanol, Propionate
Ethylene glycol	Ethylene glycol, Ethanol, Acetate



The carbon balance was subsequently calculated according to Equation 2.7.

$$\text{Carbon balance} = \frac{\sum_{j=1}^{n} \left(C_{\mathrm{P}_j, t_{\mathrm{end}}} - C_{\mathrm{P}_j, t_{\mathrm{start}}} \right)}{\sum_{i=1}^{m} \left(C_{\mathrm{S}_i, t_{\mathrm{start}}} - C_{\mathrm{S}_i, t_{\mathrm{end}}} \right)} \tag{2.7}$$

where:
$C_{\mathrm{P}_j, t}$ = Carbon concentration of product j at time t
$C_{\mathrm{S}_i, t}$ = Carbon concentration of substrate i at time t
m = Number of substrates
n = Number of products
t_{start} = Initial sampling time
t_{end} = Final sampling time

CHAPTER 3

Results and Evaluation

3.1 Construction of the CRISPR array plasmid

The transformation of the spacer plasmids into *E. coli* was verified by colony PCR and agarose gel electrophoresis . For spacer 2 (see Figure 3.1), bands were observed at the expected size (364 bp); however, the PCR products were unspecific. Colonies 1, 2, and 4 were sequenced, confirming that spacer 2 was correctly integrated into the genome. Colony 4 was selected for further use. In contrast, no bands of the correct size were detected for spacer 1 (see Figure 3.2), and sequencing confirmed unsuccessful integration. Consequently, spacer 1 was discarded.

The amplification of the homologous regions LHA and RHA from the genome of *A. woodii*, as well as the promoters pta (from *C. ijungdahlii*) and rso5 (A. woodii), was verified by agarose gel electrophoresis (see Figure 3.3). Successful amplification was confirmed by the presence of bands at approximately 1500 bp corresponding to LHA (1514 bp) and RHA (1443 bp), and bands at approximately 200 bp corresponding to the pta promoter (222 bp) and rso5 promoter (122 bp).

The next step involved the insertion of the homologous regions and the new promoters. Colony PCR and agarose gel electrophoresis revealed that only the transformation of pta-promoter plasmid was successful. For the pta-promoter, three bands were observed, but only one band at the expected size of approximately 3.8 kbp was present, which was subsequently excised and sequenced (see Figure 3.4). This colony was then used for plasmid isolation via midiprep. Although the rso5-promoter plasmid was later transformed, sequencing revealed a mutation in the alcohol dehydrogenase gene. Due to uncertainty regarding whether the error occurred during PCR or sequencing, and since the pta-promoter was already successfully transformed into *A. woodii*, the decision was made to discard the rso5-promoter construct.

The isolated plasmid DNA was measured with the NanoDrop 2000 spectrophotometer (Thermo Fisher Scientific) at a concentration of 3158 ng/µL. The purity ratios were A260/A280 = 1.84 and A260/A230 = 2.09, both within the optimal range for pure DNA, indicating minimal contamination with proteins or salts. The obtained concentration was considerably higher than the amount typically required for transformation, ensuring sufficient material for all subsequent steps.

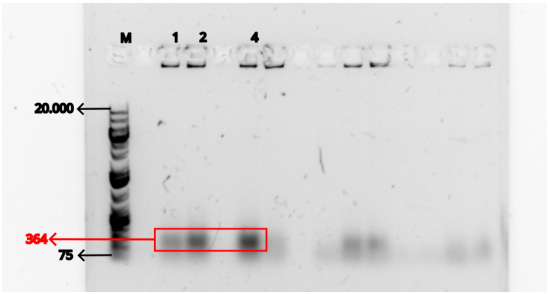


Figure 3.1: Agarose gel electrophoresis showing unspecific bands in the expected size range for Spacer 2 in all colonies, with colonies 1, 2, and 4 (marked in red) showing strong band intensity. GeneRuler 1 kb Plus DNA Ladder (Thermo Scientific) was used as a size reference (lane M).

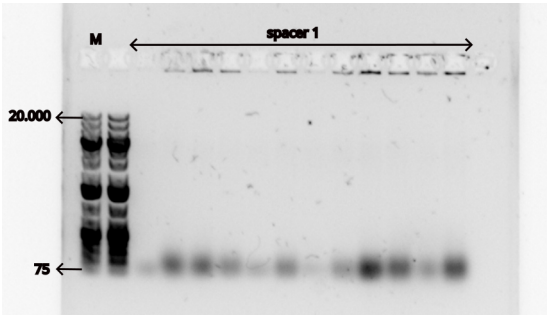


Figure 3.2: Agarose gel electrophoresis showing only primer-dimers, with no bands in the expected size range for Spacer 1. GeneRuler 1 kb Plus DNA Ladder (Thermo Scientific) was used as a size reference (lane M).

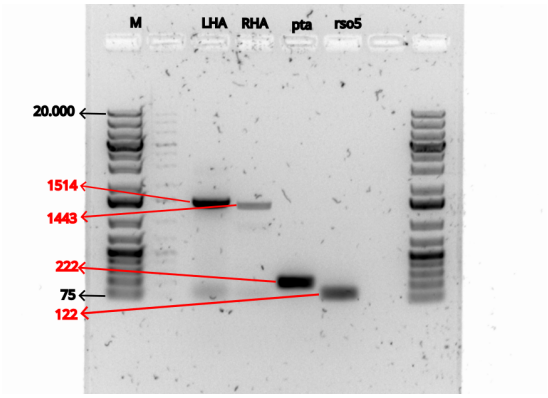


Figure 3.3: Agarose gel electrophoresis showing successful amplification of homologous regions LHA and RHA from *A. woodii* genome, and promoters pta (from *C. ijungdahlii*) and rso5 (A. woodii). Amplified bands are highlighted in red. GeneRuler 1 kb Plus DNA Ladder (Thermo Scientific) was used as a size reference (lane M).

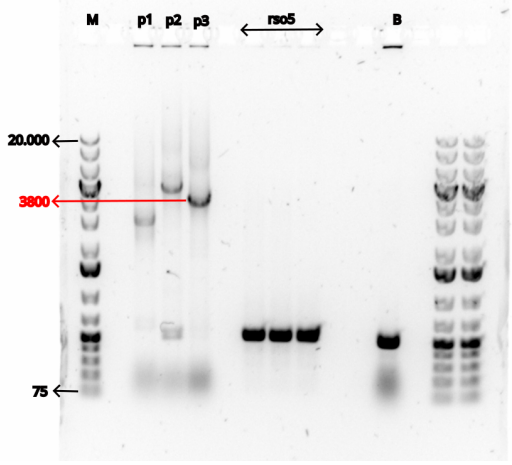


Figure 3.4: Agarose gel electrophoresis of colony PCR products. Lanes 2 and 3 show E. coli colonies containing the pta promoter, with unspecific bands. Lane 4 shows a colony with the pta promoter at the expected size. Lanes 6, 7, and 8 correspond to colonies with the rso5 promoter, which showed no bands at the expected size. Lane 10 is the negative control. GeneRuler 1 kb Plus DNA Ladder (Thermo Scientific) was used as a size reference (lane M).

3.2 Transformation of the CRISPR array plasmid into *A. woodii*

As shown in Figure 3.5, colonies 2, 4, 5, 6, 9, 10, and 12 exhibited clear and distinct bands at approximately 1600 base pairs, consistent with the expected size of the PCR-amplified pta promoter fragment. To verify whether any wild-type strains were still present among the colonies, an additional PCR was performed by the project supervisor.

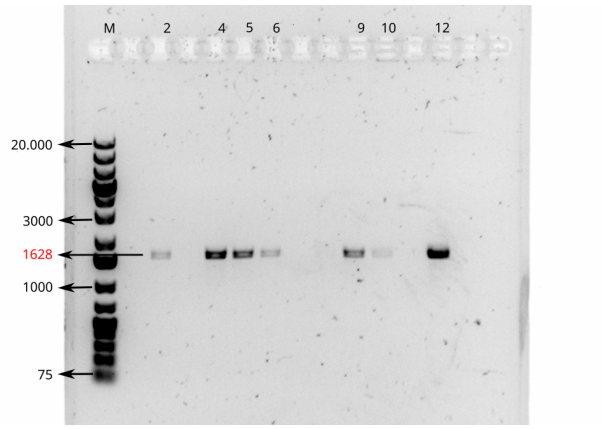
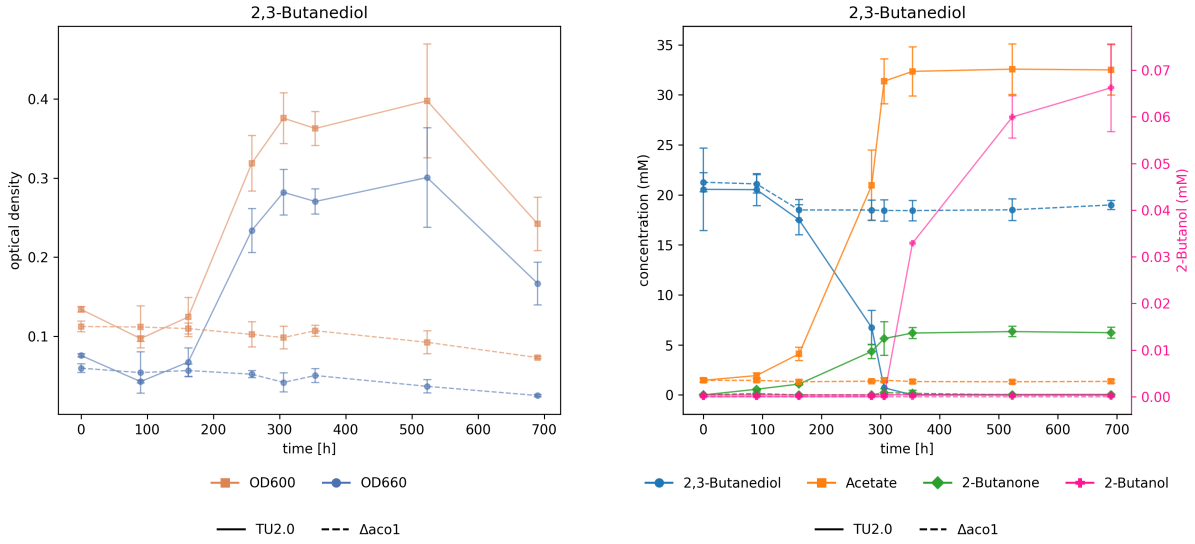


Figure 3.5: Agarose gel electrophoresis of PCR products targeting the pta promoter. Colonies 2, 4, 5, 6, 9, 10, and 12 show bands at 1600 bp, indicating successful amplification. GeneRuler 1 kb Plus DNA Ladder (Thermo Scientific) was used as a size reference (lane M).

3.3 Serum Bottle Experiments for 2-butanol Production Analysis

3.3.1 TU2.0 and Δaco1 under N_2/CO_2

2,3-Butanediol as Substrate

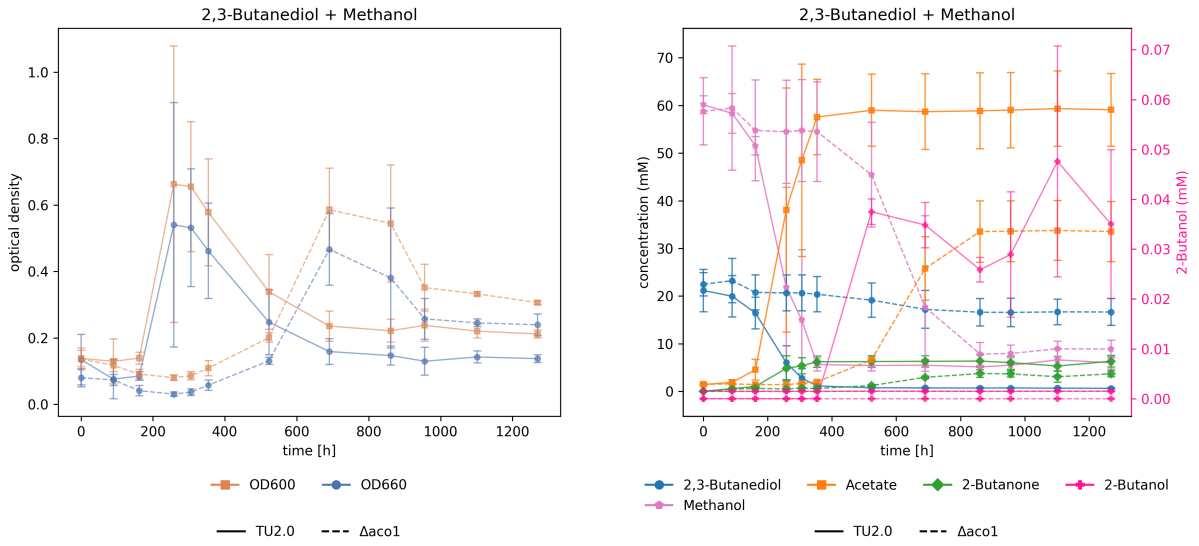


(a) $OD_{600/660}$ (b) Metabolite concentrations (HPLC)

Figure 3.6: Growth curves and metabolite concentrations for *A. woodii* TU2.0 and Δaco1 under 2,3-butanediol in a N_2/CO_2 atmosphere. Values represent the mean ± standard deviation of three independent cultures.

As shown in Figure 3.6 (b), the wild-type strain (TU2.0) converted 2,3-butanediol to 2-butanone and acetate, as expected. In both strains, the concentration of 2,3-butanediol was initially elevated. In the knockout strain, the concentration stabilized only after approximately 162 h at around 20 mM, for reasons that remain unclear. As anticipated, the knockout strain did not produce 2-butanone and acetate. In the wild type, 2-butanol was detected for the first time after 354 h of reaction time. The reaction was completed after 690 h, resulting in a final concentration of 0.0662 ± 0.0094 mM 2-butanol (mean ± SD, $n = 3$). Optical density measurements at 600 nm and 660 nm (Figure 3.6 (a)) indicated that cell growth had ceased between approximately 523 h and 690 h, consistent with the end of the reaction period.

2,3-Butanediol and Methanol as Substrates



(a) $OD_{600/660}$ (b) Metabolite concentrations (HPLC)

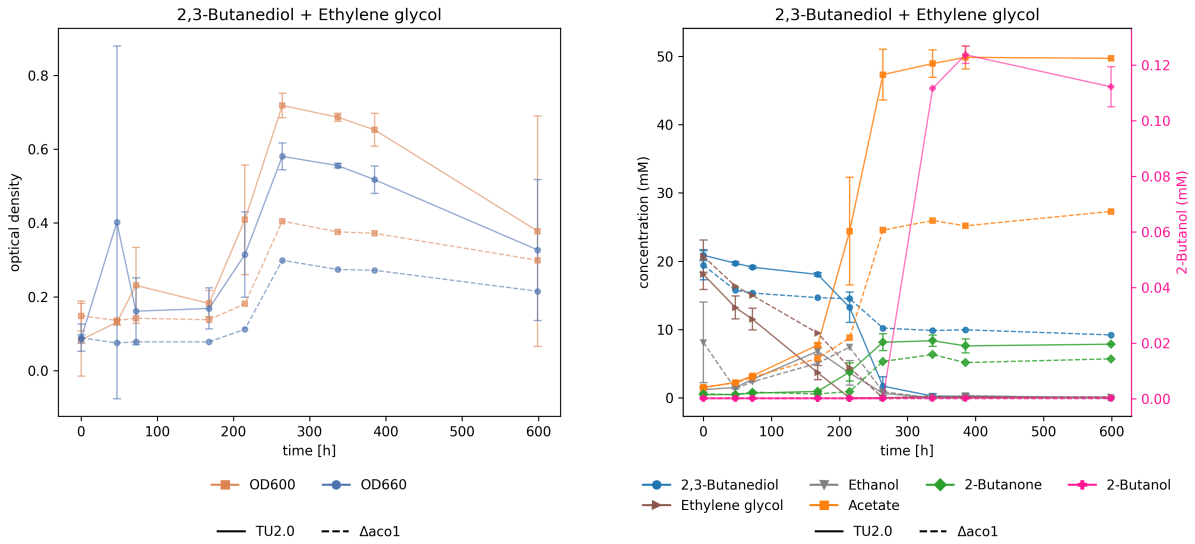
Figure 3.7: Growth curves and metabolite concentrations for *A. woodii* TU2.0 and Δaco1 under 2,3-butanediol and methanol in a N_2/CO_2 atmosphere. Values represent the mean ± standard deviation of three independent cultures.

As shown in Figure 3.7 (b), both 2,3-butanediol and methanol were metabolized to acetate by the wild-type strain. In contrast, Δaco1 utilized only methanol, with small amounts (4 mM) of 2-butanone detected, possibly due to contamination. The methanol concentration in the medium was approximately 60 mM instead of the intended 50 mM.

Optical density measurements (Figure 3.7 (a)) indicated that the reaction proceeded significantly faster in the wild-type strain compared to Δaco1. Cell growth in the wild-type ceased between 354 and 523 h, while Δaco1 reached maximum optical density only at 691 h.

As expected, only the wild-type strain produced measurable amounts of 2-butanol, with a final concentration of 0.0350±0.0150 mM (mean ± standard deviation, n=3).

2,3-Butanediol and Ethylene glycol as Substrates



(a) $OD_{600/660}$ (b) Metabolite concentrations (HPLC)

Figure 3.8: Growth curves and metabolite concentrations of A. woodii TU2.0 and Δaco1 grown with 2,3-butanediol and ethylen glycol in a N_2/CO_2 atmosphere. Values represent the mean ± standard deviation of two independent cultures, except for Δaco1, where only one culture is shown due to oxygen contamination in the other culture.

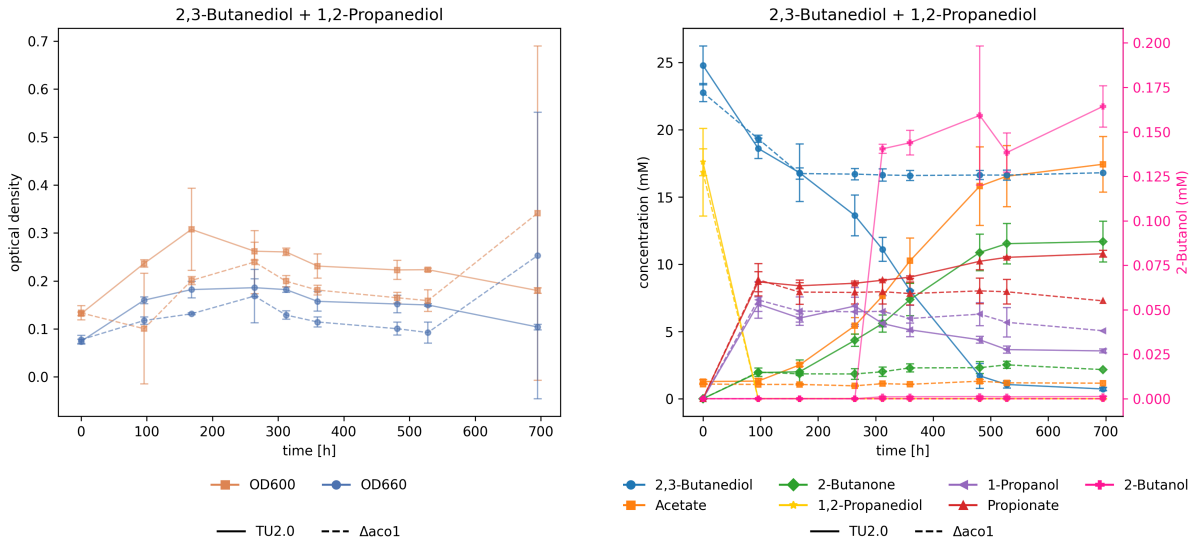
In the wild-type strain, as expected, 2,3-butanediol was co[illegible]ed to 2-butanone and acetate. In the Δaco1 strain, the conversion of 2,3-butanediol to 2-butanone and acetate was absent, as anticipated.

In the wild-type strain, ethylene glycol (EG) was metabolized to ethanol, which subsequently served as a C_1 [illegible]ce and was further converted to acetate. In the Δaco1 strain, EG was also metabolized to ethanol, which was subsequently converted to acetate. Notably, one serum bottle of the Δaco1 cultures was contaminated with oxygen, and an outlier in the ethanol concentration was observed at the beginning of the reaction due to ethanol disinfection of the serum bottle prior to sampling.

As expected, only the wild-type strain produced measurable amounts of 2-butanol, with a final concentration of 0.1122 ± 0.00720 mM (mean ± standard deviation, n=2) (Figure 3.8 (b)).

An outlier in the OD_{660} measurement of the wild-type was observed at 46 h of reaction time. In both the wild-type and the Δaco1 knockout strain, cell growth started between 72 h and 168 h and ceased between 337 h and 385 h (Figure 3.8 (a)).

2,3-Butanediol and 1,2-Propanediol as Substrates



(a) $OD_{600/660}$ (b) Metabolite concentrations (HPLC)

Figure 3.9: Growth curves and metabolite concentrations for *A. woodii* TU2.0 and Δaco1 under 2,3-butanediol and 1,2-propanediol in a N_2/CO_2 atmosphere. Values represent the mean ± standard deviation of two independent cultures.

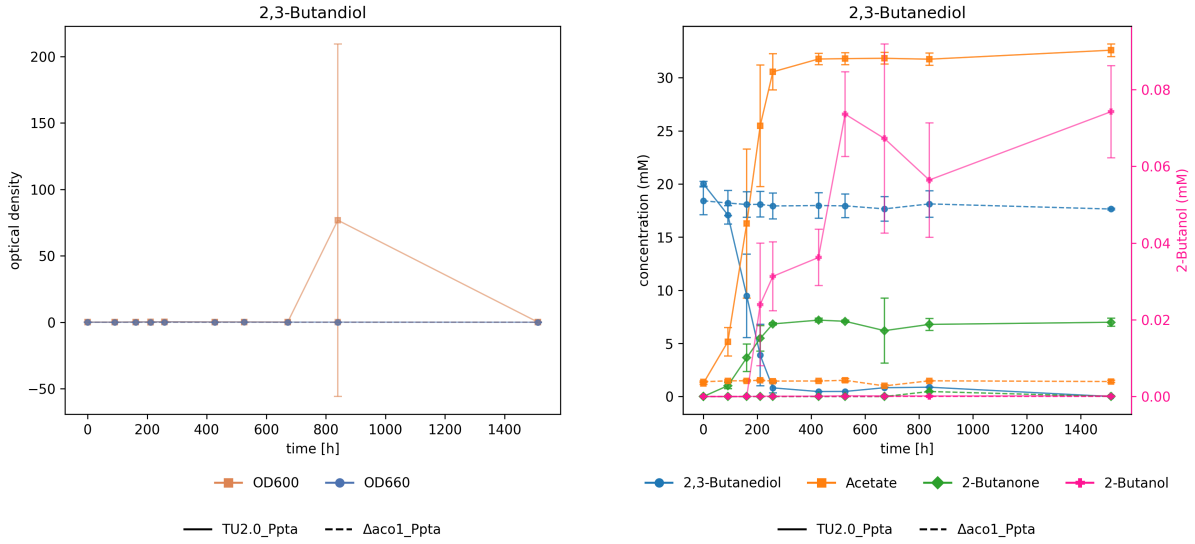
In the wild-type strain, 2,3-butanediol was converted to 2-butanone and acetate, as observed in the previous experiments. For 1,2-propanediol, both strains metabolized the substrate as expected, yielding 1-propanol and propionate in approximately equal amounts via propanal as an intermediate. Propanal itself was not detected in either the TU2.0 or the Δaco1 strain.

As expected, the production of 2-butanol was higher than in the experiments with the other substrates, with a final concentration of 0.1643 ± 0.0082 mM (mean ± standard deviation, n=2) (Figure 3.9 (b)).

The $OD_{600/660}$ measurements did not reveal clear trends or strain-specific differences in cell growth for this experiment Figure 3.9 (a)).

3.3.2 TU2.0_Ppta and Δaco1_Ppta under N_2/CO_2

2,3-Butanediol as Substrate

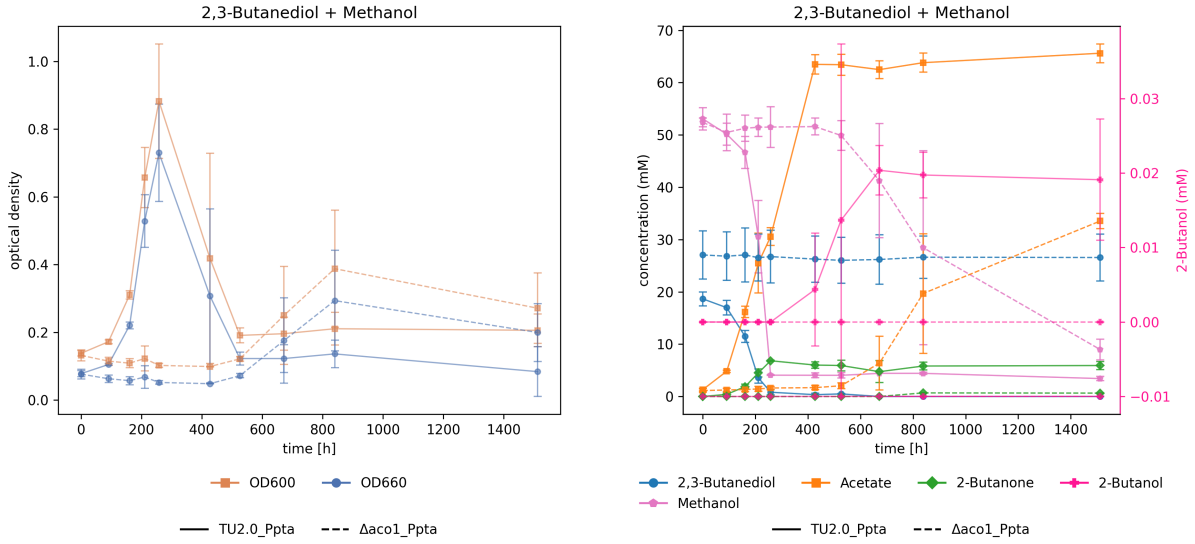


(a) $OD_{600/660}$ (b) Metabolite concentrations (HPLC)

Figure 3.10: Growth curves and metabolite concentrations for *A. woodii* TU2.0_Ppta and Δaco1_Ppta under 2,3-butanediol in a N_2/CO_2 atmosphere. Values represent the mean ± standard deviation of three independent cultures.

For the Ppta strains, the metabolic patterns for 2,3-butandiol were identical to those of the corresponding control strains, with no observable differences in either substrate consumption or product formation, including 2-butanol production. The TU2.0_Ppta OD_{600} curve contains an outlier (see Discussion). (Figure 3.10 (a) and (b)).

2,3-Butanediol and Methanol as Substrates



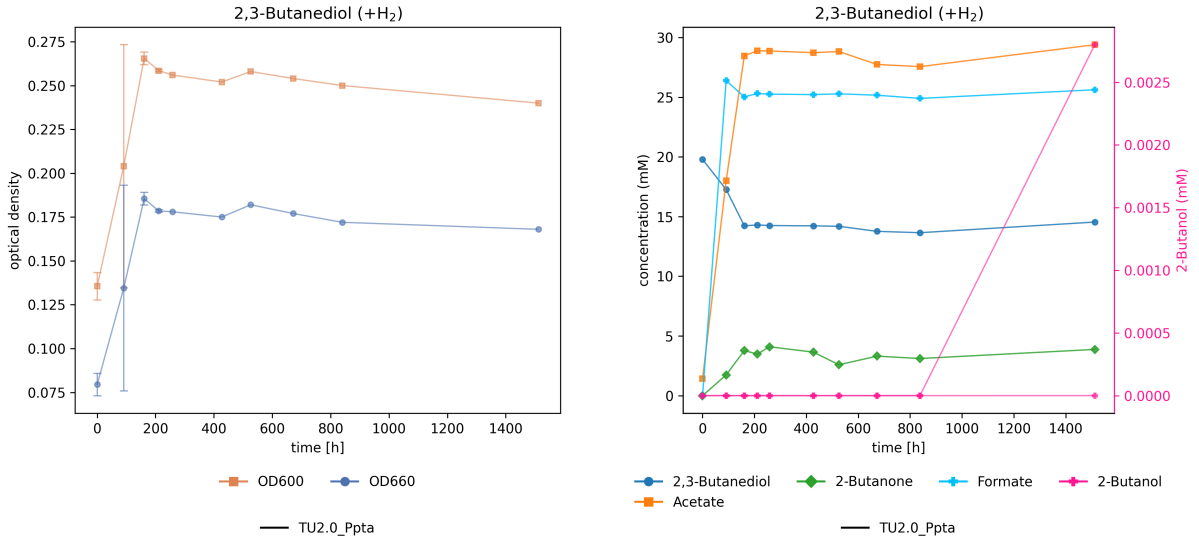
(a) $OD_{600/660}$ (b) Metabolite concentrations (HPLC)

Figure 3.11: Growth curves and metabolite concentrations for *A. woodii* TU2.0_Ppta and Δaco1_Ppta under 2,3-butanediol and methanol in a N_2/CO_2 atmosphere. Values represent the mean ± standard deviation of three independent cultures.

Similarly, for 2,3-butanediol and methanol, the stronger pta promoter had no effect on the reduction of 2,3-butanediol to 2-butanol (Figure 3.11 (a) and (b)).

3.3.3 TU2.0_Ppta under H_2

2,3-Butanediol as Substrate

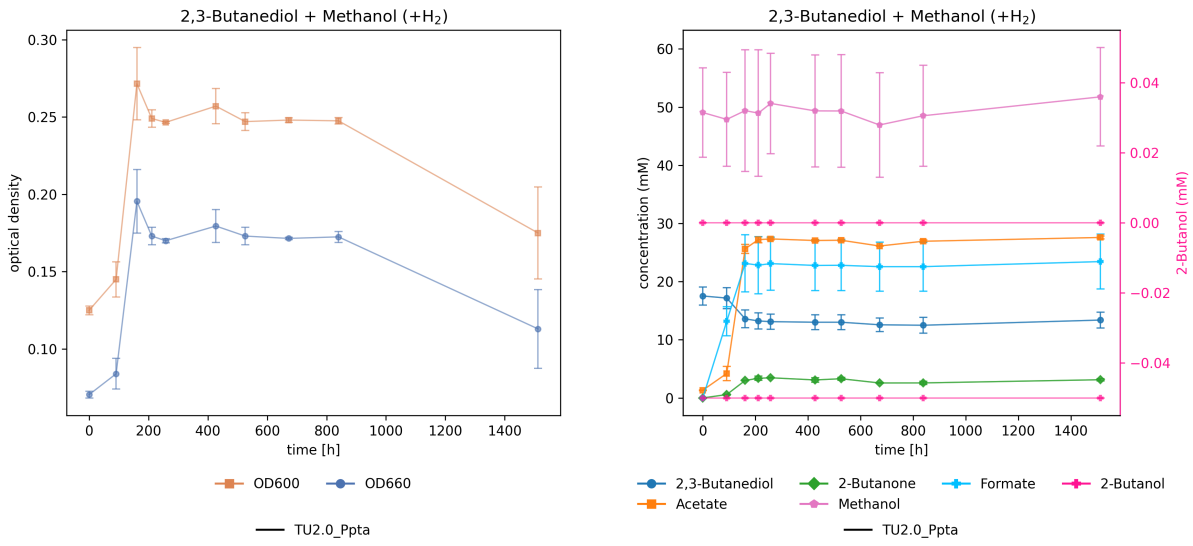


(a) $OD_{600/660}$ (b) Metabolite concentrations (HPLC)

Figure 3.12: Growth curves and metabolite concentrations for *A. woodii* TU2.0_Ppta under 2,3-butanediol in a H_2 atmosphere. Single measurement from one culture; other replicates were excluded due to oxygen contamination.

Minimal reduction of 2,3-butanediol to 2-butanone was observed; however, some 2-butanol was still produced. Substantial amounts of acetate and formate (see Discussion) were formed compared to previous experiments conducted under N_2/CO_2 conditions (Figures 3.12 (a) and (b)). One sample was excluded from analysis due to oxygen contamination.

2,3-Butanediol and Methanol as Substrates

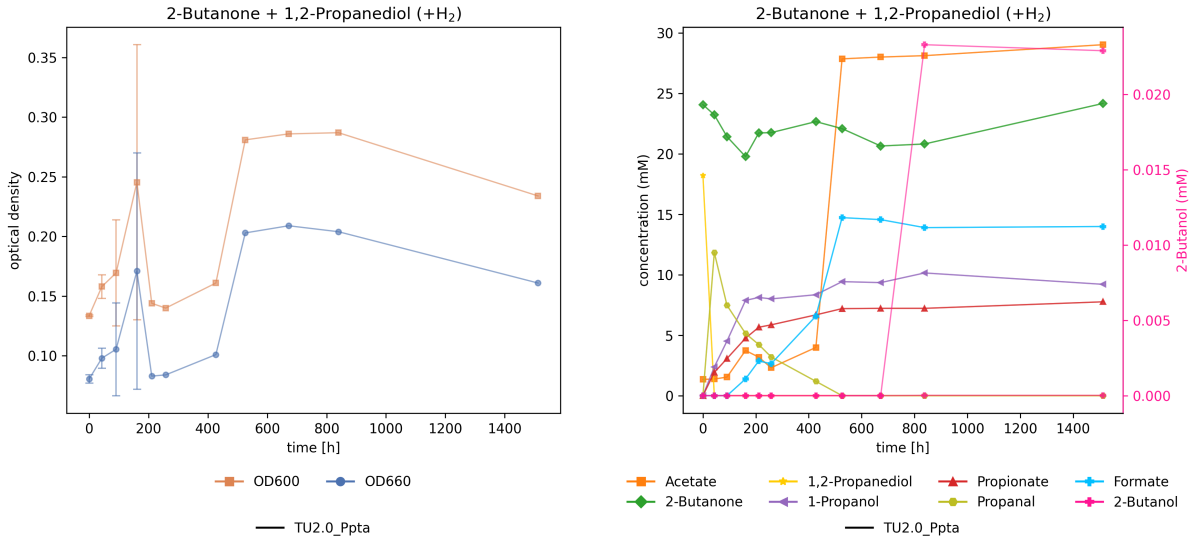


(a) $OD_{600/660}$ (b) Metabolite concentrations (HPLC)

Figure 3.13: Growth curves and metabolite concentrations for *A. woodii* TU2.0_Ppta under 2,3-butanediol and methanol in a H_2 atmosphere. Single measurement from one culture; other replicates were excluded due to oxygen contamination.

The observed behavior, as illustrated in Figure 3.13 (a) and (b), was analogous to that described for 2,3-butanediol (Section 3.3.3).

2-Butanone and 1,2-Propanediol as Substrates



(a) $OD_{600/660}$ (b) Metabolite concentrations (HPLC)

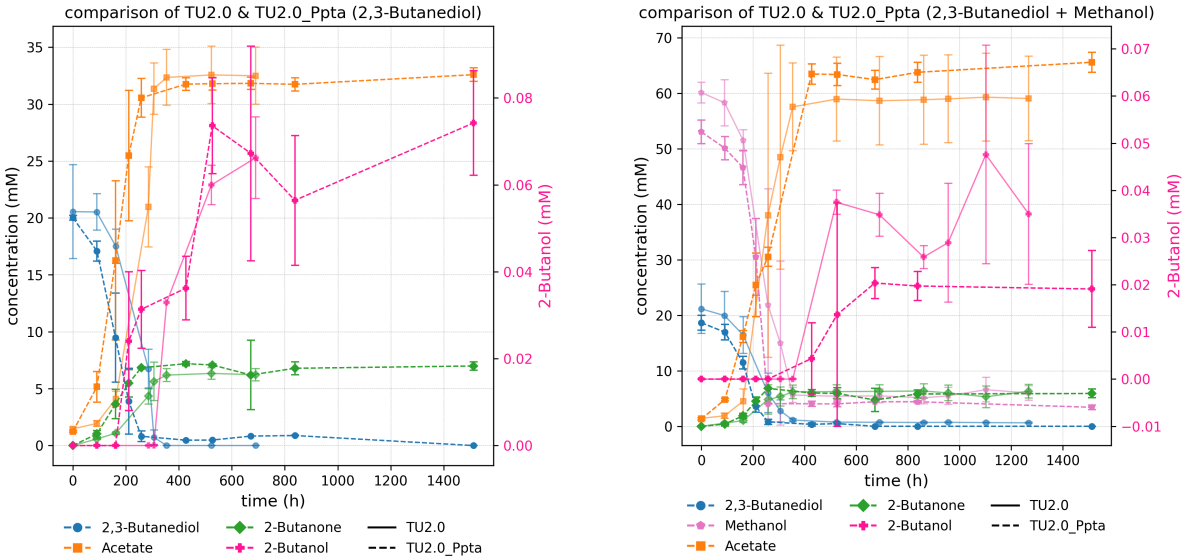
Figure 3.14: Growth curves and metabolite concentrations for *A. woodii* TU2.0_Ppta under 2-butanone and 1,2-propanediol in a H_2 atmosphere. Single measurement from one culture; other replicates were excluded due to oxygen contamination.

Similar behavior to the other experiments was observed. However, the reduction of 1,2-propanediol to 1-propanol and propionate was strongly inhibited. The intermediate propanal was detected for

approximately 427 hours before it was fully reduced to 1-propanol and propionate (Figures 3.14 (a) and (b)). One sample was excluded from analysis due to oxygen contamination.

3.3.4 Comparison of Strain Performance on 2,3-Butanediol and 2,3-Butanediol and Methanol

A direct comparison between TU2.0, TU2.0_Ppta, and Δaco1 is only possible on 2,3-butanediol and 2,3-butanediol with methanol, since these are the only shared substrates.

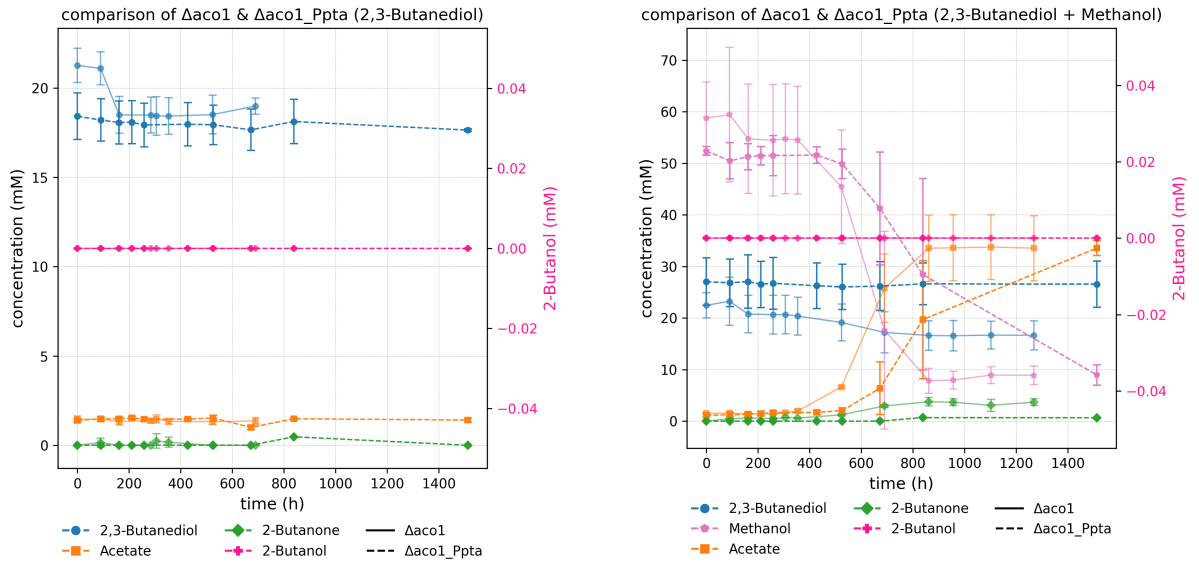


(a) 2,3-butanediol

(b) 2,3-butanediol and methanol

Figure 3.15: Comparison of metabolite production between *A. woodii* TU2.0 and TU2.0_Ppta, analyzed by HPLC under (a) 2,3-butanediol and (b) 2,3-butanediol + methanol in a N_2/CO_2 atmosphere. Values represent the mean ± standard deviation of three biological replicates.

Figure 3.15 (a) and (b) shows the course of the enzymatic degradation of 2,3-butanediol and 2,3-butanediol with methanol as a co-substrate, respectively, comparing TU2.0 and TU2.0_Ppta. Both profiles are nearly identical, indicating that the stronger pta promoter has no significant effect on the reduction of 2-butanone to 2-butanol.



(a) 2,3-butanediol

(b) 2,3-butanediol and methanol

Figure 3.16: Comparison of metabolite production between *A. woodii* Δaco1 and Δaco1_Ppta, analyzed by HPLC under (a) 2,3-butanediol and (b) 2,3-butanediol + methanol in a N_2/CO_2 atmosphere. Values represent the mean ± standard deviation of two biological replicates.

Figure 3.16 (a) and (b) illustrates the enzymatic degradation profiles for the Δaco1 strains under the same conditions. Similarly, the data show no significant difference between the strains with and without the stronger pta promoter, confirming that the promoter strength does not influence the reduction process in the Δaco1 background.

3.3.5 Carbon Recovery and Mass Balance

Figure 3.3.5 shows the total carbon balance of all experiments. The red dashed line at 1.0 represents the ideal carbon balance, i.e., the condition in which all carbon entering the reaction is recovered in the measured products. This ideal was met in experiments 4 to 10. In contrast, experiments 1 to 3, representing reduction attempts under H_2, exhibited carbon recoveries well above the ideal value due to additional carbon from acetate and formate. Notably, experiments 2 and 3 showed nearly five times the carbon output relative to the input. Experiments 11 to 13, however, displayed carbon deficits, with less carbon recovered than initially supplied.

No carbon balance was determined for 2,3-butanediol with the Δaco1 (see Figure 3.6 (b)) and Δaco1_Ppta (see Figure 3.10 (b)) strains, as 2,3-butanediol was not metabolized to acetate and 2-butanone in these strains.

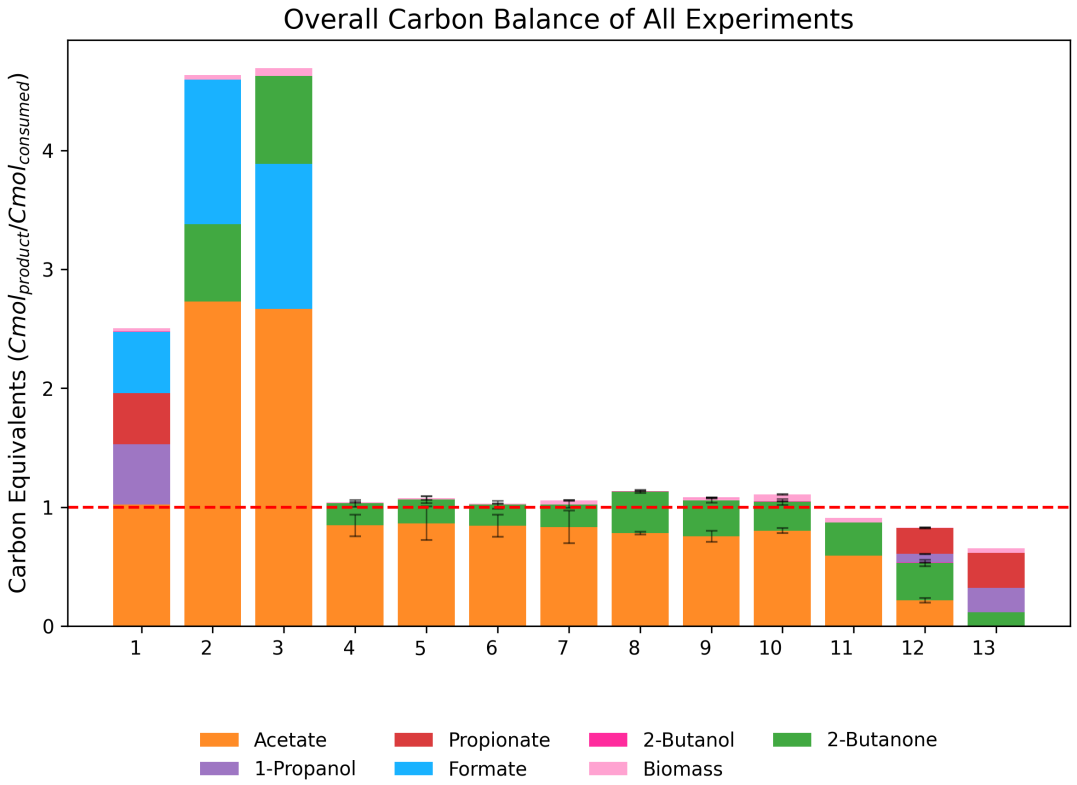


Figure 3.17: Total carbon balance of all experiments. Bars are numbered as follows: 1) 2-butanone + 1,2-propanediol (TU2.0_Ppta under H_2), 2) 2,3-butanediol + MeOH (TU2.0_Ppta under H_2), 3) 2,3-butanediol (TU2.0_Ppta under H_2), 4) 2,3-butanediol + MeOH (TU2.0_Ppta), 5) 2,3-butanediol + MeOH (Δaco1_Ppta), 6) 2,3-butanediol + MeOH (TU2.0), 7) 2,3-butanediol + MeOH (Δaco1), 8) 2,3-butanediol (TU2.0_Ppta), 9) 2,3-butanediol (TU2.0), 10) 2,3-butanediol + ethylene glycol (TU2.0), 11) 2,3-butanediol + ethylene glycol (Δaco1), 12) 2,3-butanediol + 1,2-propanediol (TU2.0), 13) 2,3-butanediol + 1,2-propanediol (Δaco1).

CHAPTER 4

Discussion

4.1 Promoter Exchange of ADH4 in *A. woodii*

One objective of this study was to replace the promoter of ADH4 with a stronger promoter (PTA or RSO5) to enhance the production of 2-butanol. For this purpose, two different CRISPR spacers were provided as a backup strategy.

Of the two spacers, only Spacer 2 was successfully utilized; Spacer 1 could not be integrated into the CRISPR system despite multiple attempts. A plausible explanation is that Spacer 1 either binds inefficiently to the target sequence [SJD+11, WvDB+11] or that the DNA structure at this location hinders a successful CRISPR/Cas interaction [ZHA+13, MKKK19]. Technical issues in plasmid construction or low activity of the Cas component at this position may also play a role [MB13, BSM+15, MKB+19].

The PTA promoter was successfully transformed into *A. woodii*. The incorporation of the RSO5 promoter was not performed, as a mutation in the adh4 sequence was discovered during preparation. It is more likely that this mutation occurred during PCR amplification, as sequencing errors in modern methods are relatively rare [CBG+20, MAH14]. To avoid potential sources of error, transformation with RSO5 was therefore omitted.

Analysis of 2-butanol production showed no increase with the introduced PTA promoter. This suggests that the limitation is not in the expression of ADH4 but is likely determined by other factors in the metabolism, such as the redox balance ($NADH/NAD^+$) or the flux in the Wood–Ljungdahl pathway.

Overall, it is evident that a stronger promoter alone is insufficient to increase 2-butanol production.

4.2 Effect of 1,2-Propanediol on 2-Butanol Formation

Within the scope of this work, it was investigated whether 1,2-propanediol (1,2-PD) as a co-substrate influences the reduction of 2-butanone to 2-butanol in *A. woodii* via PduQ. The results demonstrated that the addition of 1,2-PD indeed promotes 2-butanol formation.

Although the behavior of 1,2-PD in A. woodii has not been previously described, evidence from other bacteria, such as Salmonella enterica, indicates a potential mechanism. In S. enterica [CFSB12], the alcohol dehydrogenase PduQ plays a central role in $NADH/NAD^+$ recycling within a bacterial microcompartment (Pdu MCP), thereby supplying cofactors for the dehydrogenase. This suggests that the effect of 1,2-PD on 2-butanol formation in A. woodii is mediated via PduQ.

These results support the hypothesis that 1,2-PD as a co-substrate facilitates PduQ-catalyzed reduction of 2-butanone to 2-butanol.

4.3 Carbon balance of mixed-substrate fermentations

As shown in Section 3.3.5 and Figure 3.3.5, most of the carbon balances were close to 100 %, except for three cases measured under N_2/CO_2 conditions, which fell below full recovery: 2,3-butanediol + ethylene glycol (Δaco1, 90 %), 2,3-butanediol + 1,2-propanediol (TU2.0, 82 %), and 2,3-butanediol + 1,2-propanediol (Δaco1, 65%). Carbon balances under H_2 atmosphere were generally above 100 % (see section 4.4).

The missing fraction of carbon can be explained by several factors: (i) volatile intermediates (e.g., aldehydes or ketones) that escape into the gas phase and are not captured by HPLC, (ii) dissolved inorganic carbon (DIC) that was not quantified, (iii) uncertainties in estimating biomass carbon via OD/CDW conversions, and (iv) minor volume losses due to evaporation or sampling.

The most likely forms of unaccounted DIC are dissolved carbon dioxide (CO_2(aq)) and its hydration product, bicarbonate (HCO_3^-). These species are natural end-products of the incomplete oxidation of organic substrates and can accumulate if not fully assimilated by the Wood-Ljungdahl pathway under the given conditions. Similar limitations in carbon balances are a common challenge in diverse biological systems. For instance, in the dark ocean, the omission of dark inorganic carbon fixation (DIC_{fix}) rates led to a significant underestimation of carbon supply [RBSV+25]. This underscores that the failure to account for all inorganic carbon pools is a common and major source of error in carbon mass balance calculations.

4.4 Hypothesis on the Preferential Use of the Wood-Ljungdahl Pathway under H_2 Conditions

As shown in Section 3.3.5 and Figure 3.3.5, most carbon recoveries were close to 100 %, with the exception of three cases under N_2/CO_2 conditions that fell below full recovery. In contrast, the apparent carbon recoveries under H_2 conditions substantially exceeded the input, reaching 469 % for 2,3-butanediol (TU2.0_Ppta), 459 % for 2,3-butanediol + methanol (TU2.0_Ppta), and 250 % for 2-butanone + 1,2-propanediol (TU2.0_Ppta).

These unexpectedly high values likely result from the preferential utilization of the Wood–Ljungdahl pathway (WLP) by *A. woodii* under hydrogenic conditions. The WLP enables direct incorporation of carbonate from the medium as a carbon source [RP08] and provides an energetically favorable route for acetate production, as acetate formation from H_2 and CO_2 is coupled to net ATP synthesis [Sch77]. This pathway serves as the primary metabolic route for this organism under autotrophic conditions [BM15]. Consequently, alternative substrates such as 2,3-butanediol or 1,2-propanediol may be minimally metabolized, potentially due to enzymatic inhibition or the high redox potential associated with H_2 oxidation, which could contribute to the apparent overestimation of carbon recovery in the measurements.

4.5 Challenges in HPLC quantification of 2-butanol

As shown in Section 3.3 and Figure 3.6 to 3.14, the irregular "zig-zag" pattern observed for the 2-butanol curves can be attributed to the very low amounts of product formed, which were barely recognized as 2-butanol peaks by Chromeleon. Additionally, a neighboring peak originating from a previous sample, likely due to components in the medium, co-eluted with the 2-butanol peak. This residual compound remained in the HPLC column and appeared delayed in subsequent runs. To achieve a clean separation of 2-butanol, the HPLC runtime was shortened. Consequently, the 2-butanol peaks from earlier samples were partially truncated by the adjacent larger peak during integration, resulting in the irregular peak shapes observed.

4.6 Outliers in Optical Density Measurements

Despite thorough vortexing prior to measurement, occasional outliers in OD readings were observed, notably in Figures 3.8 and 3.10. These deviations are most likely attributable to incomplete homogenization of the culture, which can lead to transient cell clumping and locally elevated cell densities. Additionally, air bubbles or foam trapped in the culture during sampling may have caused sporadic light scattering, resulting in artificially high readings. Instrumental factors, such as minor variations in the light path or condensation on the cuvette, may have further contributed to measurement variability. Finally, short-term sedimentation of cells between vortexing and measurement could have exacerbated these deviations.

To reduce such outliers in future experiments, repeated measurements, careful removal of air bubbles, and thorough homogenization immediately prior to sampling are recommended.

CHAPTER 5

Outlook

The results of this work suggest that the expression level of ADH4 is not the main limitation for 2-butanol production in *A. woodii*. Instead, the availability of reducing equivalents (NADH/NAD^+ balance) seems to play a more critical role.

Future work should therefore focus on strategies to increase NADH availability, such as modifying competing pathways, testing cofactor engineering approaches, or optimizing cultivation conditions that favor a more reduced cellular state. Additionally, redirecting flux within the Wood–Ljungdahl pathway could help provide the necessary redox power for efficient butanol formation.

Overall, this highlights that further improvements in 2-butanol production will require metabolic engineering beyond promoter strength, with special attention to redox balance and energy metabolism.

List of Figures

1.1 Schematic representation of the Wood–Ljungdahl pathway (WLP) in *A. woodii*, showing the methyl and carbonyl branches that come together in the formation of acetyl-CoA. Adapted from Klara Wögerbauer. 2

1.2 Schematic representation of the 2,3-butanediol metabolism in *A. woodii*. 2,3-butanediol is oxidized by the PduCDE complex to 2-butanone (MEK), which can be reduced to 2-butanol by PduQ (ADH4). Simultaneously, 2,3-butanediol can be converted to acetoin by budC, which is then transformed to acetaldehyde and two molecules of acetyl-CoA via Aco1. Acetaldehyde can be further oxidized to acetyl-CoA, with one acetyl-CoA molecule converted to acetate with concomitant ATP formation. Adapted from Klara Wögerbauer. 3

1.3 Schematic overview of the endogenous Type I-B CRISPR/Cas system mediated promoter replacement in *A. woodii*. A synthetic CRISPR array provides a crRNA that guides the Cascade complex to the target site next to a PAM sequence. Cas3 is then recruited and introduces a double-strand break in the genomic DNA. Homologous recombination with a donor DNA template containing the new promoter flanked by left and right homology arms (LHA and RHA) enables the integration of the modified sequence. (Adapted from a BioRender template by Esmée Dragt (biorender.com).) 4

1.4 Schematic overview of the Golden Gate cloning process. (1) Linearized plasmid and DNA inserts with designed overhangs. (2) Complementary overhangs anneal. (3) T4 DNA ligase seals the nicks, yielding the final assembled plasmid. (Adapted from a BioRender template by Samara Ona (biorender.com).) 5

2.1 Linear regression of refractive index (RI) peak areas against known 2-butanone concentrations. The resulting calibration equation allows conversion of concentrations determined from UV280 spectra into expected RI peak areas. 12

2.2 Linear regression of the calibration curve for 1-propanol, relating RI peak areas to known concentrations. The resulting regression equation enables conversion of calculated peak areas into concentrations. 12

3.1 Agarose gel electrophoresis showing unspecific bands in the expected size range for Spacer 2 in all colonies, with colonies 1, 2, and 4 (marked in red) showing strong band intensity. GeneRuler 1 kb Plus DNA Ladder (Thermo Scientific) was used as a size reference (lane M). 15

3.2 Agarose gel electrophoresis showing only primer-dimers, with no bands in the expected size range for Spacer 1. GeneRuler 1 kb Plus DNA Ladder (Thermo Scientific) was used as a size reference (lane M). 15

3.3 Agarose gel electrophoresis showing successful amplification of homologous regions LHA and RHA from *A. woodii* genome, and promoters pta (from *C. ijungdahlii*) and rso5 (A. woodii). Amplified bands are highlighted in red. GeneRuler 1 kb Plus DNA Ladder (Thermo Scientific) was used as a size reference (lane M). 15

3.4 Agarose gel electrophoresis of colony PCR products. Lanes 2 and 3 show E. coli colonies containing the pta promoter, with unspecific bands. Lane 4 shows a colony with the pta promoter at the expected size. Lanes 6, 7, and 8 correspond to colonies with the rso5 promoter, which showed no bands at the expected size. Lane 10 is the negative control. GeneRuler 1 kb Plus DNA Ladder (Thermo Scientific) was used as a size reference (lane M). 15
3.5 Agarose gel electrophoresis of PCR products targeting the pta promoter. Colonies 2, 4, 5, 6, 9, 10, and 12 show bands at 1600 bp, indicating successful amplification. GeneRuler 1 kb Plus DNA Ladder (Thermo Scientific) was used as a size reference (lane M). 16
3.6 Growth curves and metabolite concentrations for *A. woodii* TU2.0 and Δaco1 under 2,3-butanediol in a N_2/CO_2 atmosphere. Values represent the mean ± standard deviation of three independent cultures. 16
3.7 Growth curves and metabolite concentrations for *A. woodii* TU2.0 and Δaco1 under 2,3-butanediol and methanol in a N_2/CO_2 atmosphere. Values represent the mean ± standard deviation of three independent cultures. 17
3.8 Growth curves and metabolite concentrations of A. woodii TU2.0 and Δaco1 grown with 2,3-butanediol and ethylen glycol in a N_2/CO_2 atmosphere. Values represent the mean ± standard deviation of two independent cultures, except for Δaco1, where only one culture is shown due to oxygen contamination in the other culture. 18
3.9 Growth curves and metabolite concentrations for *A. woodii* TU2.0 and Δaco1 under 2,3-butanediol and 1,2-propanediol in a N_2/CO_2 atmosphere. Values represent the mean ± standard deviation of two independent cultures. 19
3.10 Growth curves and metabolite concentrations for *A. woodii* TU2.0_Ppta and Δaco1_Ppta under 2,3-butanediol in a N_2/CO_2 atmosphere. Values represent the mean ± standard deviation of three independent cultures. 20
3.11 Growth curves and metabolite concentrations for *A. woodii* TU2.0_Ppta and Δaco1_Ppta under 2,3-butanediol and methanol in a N_2/CO_2 atmosphere. Values represent the mean ± standard deviation of three independent cultures. 20
3.12 Growth curves and metabolite concentrations for *A. woodii* TU2.0_Ppta under 2,3-butanediol in a H_2 atmosphere. Single measurement from one culture; other replicates were excluded due to oxygen contamination. 21
3.13 Growth curves and metabolite concentrations for *A. woodii* TU2.0_Ppta under 2,3-butanediol and methanol in a H_2 atmosphere. Single measurement from one culture; other replicates were excluded due to oxygen contamination. 22
3.14 Growth curves and metabolite concentrations for *A. woodii* TU2.0_Ppta under 2-butanone and 1,2-propanediol in a H_2 atmosphere. Single measurement from one culture; other replicates were excluded due to oxygen contamination. 22
3.15 Comparison of metabolite production between *A. woodii* TU2.0 and TU2.0_Ppta, analyzed by HPLC under (a) 2,3-butanediol and (b) 2,3-butanediol + methanol in a N_2/CO_2 atmosphere. Values represent the mean ± standard deviation of three biological replicates. 23
3.16 Comparison of metabolite production between *A. woodii* Δaco1 and Δaco1_Ppta, analyzed by HPLC under (a) 2,3-butanediol and (b) 2,3-butanediol + methanol in a N_2/CO_2 atmosphere. Values represent the mean ± standard deviation of two biological replicates. 24
3.17 Total carbon balance of all experiments. Bars are numbered as follows: 1) 2-butanone + 1,2-propanediol (TU2.0_Ppta under H_2), 2) 2,3-butanediol + MeOH (TU2.0_Ppta under H_2), 3) 2,3-butanediol (TU2.0_Ppta under H_2), 4) 2,3-butanediol + MeOH (TU2.0_Ppta), 5) 2,3-butanediol + MeOH (Δaco1_Ppta), 6) 2,3-butanediol + MeOH (TU2.0), 7) 2,3-butanediol + MeOH (Δaco1), 8) 2,3-butanediol (TU2.0_Ppta), 9) 2,3-butanediol (TU2.0), 10) 2,3-butanediol + ethylene glycol (TU2.0), 11) 2,3-butanediol + ethylene glycol (Δaco1), 12) 2,3-butanediol + 1,2-propanediol (TU2.0), 13) 2,3-butanediol + 1,2-propanediol (Δaco1). 25

List of Tables

2.1 Ingredients for 1 L of the defined growth medium 6
2.2 Composition of 1 L undefined medium for agar plates. 7
2.3 Antibiotics used for the bacterial strains 7
2.4 Composition of 1 L undefined medium 7
2.5 Codes and details for serum bottles with strains expressing native promoter (strain and carbon source). 10
2.6 Codes and details for serum bottles with transformed *A. woodii* strains expressing the *pta* promoter (strain and carbon source). 10
2.7 Overview of relevant compounds used for carbon balancing. The number of carbon atoms per molecule was used to calculate mmol of carbon from measured concentrations. . . 12
2.8 Assumed carbon flow from substrate compounds to observed products for carbon balancing. 13

1 Preparation of HPLC standards. 37
2 Verwendete Primer für die PCR 38

Bibliography

[BM15] Johannes Bertsch and Volker Müller. Co metabolism in the acetogen acetobacterium woodii. *Applied and Environmental Microbiology*, 81(17):5949–5956, 2015.

[BSM+15] Pierre Boudry, Ekaterina Semenova, Marc Monot, Kirill A. Datsenko, Anna Lopatina, Ognjen Sekulovic, Maicol Ospina-Bedoya, Louis-Charles Fortier, Konstantin Severinov, Bruno Dupuy, and Olga Soutourina. Function of the crispr-cas system of the human pathogen clostridium difficile. *mBio*, 6(5):10.1128/mbio.01112–15, 2015.

[BSTW77] W.E. Balch, S. Schoberth, R.S. Tanner, and R.S. Wolfe. Methanogenic bacteria: characterization of an unusual anaerobic group of bacteria. *International Journal of Systematic Bacteriology*, 27(4):355–361, 1977.

[CBG+20] Beate M. Crossley, Jianfa Bai, Amy Glaser, Roger Maes, Elizabeth Porter, Mary Lea Killian, Travis Clement, and Kathy Toohey-Kurth. Guidelines for sanger sequencing and molecular assay monitoring. *Journal of Veterinary Diagnostic Investigation*, 32(6):767–775, 2020. PMID: 32070230.

[CFSB12] Shouqiang Cheng, Chenguang Fan, Sharmistha Sinha, and Thomas A. Bobik. The pduq enzyme is an alcohol dehydrogenase used to recycle nad+ internally within the pdu microcompartment of salmonella enterica. *PLOS ONE*, 7(10):1–11, 10 2012.

[Deb21] V. G. Debabov. Acetogens: Biochemistry, bioenergetics, genetics, and biotechnological potential. *Microbiology*, 90(3):273–297, 2021.

[Die92] G. Diekert. Acetogenic bacteria. In A. Balows, H.G. Trüper, M. Dworkin, W. Harder, and K.-H. Schleifer, editors, *The Prokaryotes*, pages 517–533. Springer-Verlag, New York, 1992.

[Dra94] Harold L. Drake. *Acetogenesis, Acetogenic Bacteria, and the Acetyl-CoA "Wood/Ljungdahl" Pathway: Past and Current Perspectives*, pages 3–60. Springer US, Boston, MA, 1994.

[DSD+87] W. Dangel, H. Schulz, G. Diekert, H. König, and G. Fuchs. Occurrence of corrinoid-containing membrane proteins in anaerobic bacteria. *Archives of Microbiology*, 148(1):52–56, 1987.

[EKM08] Carola Engler, Romy Kandzia, and Sylvestre Marillonnet. A one pot, one step, precision cloning method with high throughput capability. *PLOS ONE*, 3(11):1–7, 11 2008.

[EYG+14] Carola Engler, Mark Youles, Ramona Gruetzner, Tim-Martin Ehnert, Stefan Werner, Jonathan D. G. Jones, Nicola J. Patron, and Sylvestre Marillonnet. A golden gate modular cloning toolbox for plants. *ACS Synthetic Biology*, 3(11):839–843, 2014.

[Fuc86] Georg Fuchs. Co2 fixation in acetogenic bacteria: variations on a theme. *FEMS Microbiology Reviews*, 2(3):181–213, 1986.

[GLR90] Andrew R. Godley, Paul E. Linnett, and John P. Robinson. The effect of carbon dioxide on the growth kinetics of fructose-limited chemostat cultures of acetobacterium woodii dsm 1030. *Archives of Microbiology*, 154(1):5–11, 1990.

[HOTM15] Verena Hess, Olga Oyrik, Dragan Trifunović, and Volker Müller. 2, 3-butanediol metabolism in the acetogen acetobacterium woodii. *Applied and Environmental Microbiology*, 81(14):4711–4719, 2015.

[Lju86] L G Ljungdhal. The autotrophic pathway of acetate synthesis in acetogenic bacteria. *Annual Review of Microbiology*, 40(Volume 40,):415–450, 1986.

[MAH14] Peter McInerney, Paul Adams, and Masood Z. Hadi. Error rate comparison during polymerase chain reaction by dna polymerase. *Molecular Biology International*, 2014(1):287430, 2014.

[Mar20] William F. Martin. Older than genes: The acetyl coa pathway and origins. *Frontiers in Microbiology*, 11:817, 2020.

[MB13] Sabin Mulepati and Scott Bailey. In vitro reconstitution of an escherichia coli rna-guided immune system reveals unidirectional, atp-dependent degradation of dna target*. *Journal of Biological Chemistry*, 288(31):22184–22192, 2013.

[MKB+19] Anna Maikova, Victor Kreis, Anaïs Boutserin, Konstantin Severinov, and Olga Soutourina. Using an endogenous crispr-cas system for genome editing in the human pathogen clostridium difficile. *Applied and Environmental Microbiology*, 85(20):e01416–19, 2019.

[MKKK19] Su Bin Moon, Do Yon Kim, Jeong-Heon Ko, and Yong-Sam Kim. Recent advances in the crispr genome editing tool set. *Experimental & Molecular Medicine*, 51(11):1–11, 2019.

[NVD+21] Christian Simon Neuendorf, Gabriel A. Vignolle, Christian Derntl, Tamara Tomin, Katharina Novak, Robert L. Mach, Ruth Birner-Grünberger, and Stefan Pflügl. A quantitative metabolic analysis reveals acetobacterium woodii as a flexible and robust host for formate-based bioproduction. *Metabolic Engineering*, 68:68–85, 2021.

[OSS91] F B Oppermann, B Schmidt, and A Steinbüchel. Purification and characterization of acetoin:2,6-dichlorophenolindophenol oxidoreductase, dihydrolipoamide dehydrogenase, and dihydrolipoamide acetyltransferase of the pelobacter carbinolicus acetoin dehydrogenase enzyme system. *Journal of Bacteriology*, 173(2):757–767, 1991.

[PDBM+23] Margaux Poulalier-Delavelle, Jonathan P. Baker, James Millard, Klaus Winzer, and Nigel P. Minton. Endogenous crispr/cas systems for genome engineering in the acetogens acetobacterium woodii and clostridium autoethanogenum. *Frontiers in Bioengineering and Biotechnology*, Volume 11 - 2023, 2023.

[POM+15] Nicola J. Patron, Diego Orzaez, Sylvestre Marillonnet, Heribert Warzecha, Colette Matthewman, Mark Youles, Oleg Raitskin, Aymeric Leveau, Gemma Farré, Christian Rogers, Alison Smith, Julian Hibberd, Alex A. R. Webb, James Locke, Sebastian Schornack, Jim Ajioka, David C. Baulcombe, Cyril Zipfel, Sophien Kamoun, Jonathan D. G. Jones, Hannah Kuhn, Silke Robatzek, H. Peter Van Esse, Dale Sanders, Giles Oldroyd, Cathie Martin, Rob Field, Sarah O'Connor, Samantha Fox, Brande Wulff, Ben Miller, Andy Breakspear, Guru Radhakrishnan, Pierre-Marc Delaux, Dominique Loqué, Antonio Granell, Alain Tissier, Patrick Shih, Thomas P. Brutnell, W. Paul Quick, Heiko Rischer, Paul D. Fraser, Asaph Aharoni, Christine Raines, Paul F. South, Jean-Michel Ané, Björn R. Hamberger, Jane Langdale, Jens Stougaard, Harro Bouwmeester, Michael Udvardi, James A. H. Murray, Vardis Ntoukakis, Patrick Schäfer, Katherine Denby, Keith J. Edwards, Anne Osbourn, and Jim Haseloff. Standards for plant synthetic biology: a common syntax for exchange of dna parts. *New Phytologist*, 208(1):13–19, 2015.

[Rag91] Stephen W Ragsdale. Enzymology of the acetyl-coa pathway of co2 fixation. *Critical reviews in biochemistry and molecular biology*, 26(3-4):261–300, 1991.

[RBSV+25] T. Reich, N. Belkin, G. Sisma-Ventura, H. Hauzer, M. Rubin-Blum, I. Berman-Frank, and E. Rahav. Dark inorganic carbon fixation contributes to bacterial organic carbon demand in the oligotrophic southeastern mediterranean sea. *EGUsphere*, 2025:1–29, 2025.

[RP08] Stephen W. Ragsdale and Eric Pierce. Acetogenesis and the wood-ljungdahl pathway of co(2) fixation. *Biochimica et Biophysica Acta (BBA) - Proteins and Proteomics*, 1784(12):1873–1898, December 2008.

[Sch77] Siegfried Schoberth. Acetic acid from h2 and co2. *Archives of Microbiology*, 114(2):143–148, August 1977.

[SJD+11] Ekaterina Semenova, Matthijs M. Jore, Kirill A. Datsenko, Anna Semenova, Edze R. Westra, Barry Wanner, John van der Oost, Stan J. J. Brouns, and Konstantin Severinov. Interference by clustered regularly interspaced short palindromic repeat (crispr) rna is governed by a seed sequence. *Proceedings of the National Academy of Sciences*, 108(25):10098–10103, 2011.

[SSL+15] Kai Schuchmann, Silke Schmidt, Antonio Martinez Lopez, Christina Kaberline, Martin Kuhns, Wolfram Lorenzen, Helge B. Bode, Friederike Joos, and Volker Müller. Nonacetogenic growth of the acetogen acetobacterium woodii on 1,2-propanediol. *Journal of Bacteriology*, 197(2):382–391, 2015.

[WEG+11] Ernst Weber, Carola Engler, Ramona Gruetzner, Stefan Werner, and Sylvestre Marillonnet. A modular cloning system for standardized assembly of multigene constructs. *PLOS ONE*, 6(2):1–11, 02 2011.

[Woo91] Harland G Wood. Life with co or co2 and h2 as a source of carbon and energy. *The FASEB journal*, 5(2):156–163, 1991.

[WvDB+11] Blake Wiedenheft, Esther van Duijn, Jelle B. Bultema, Sakharam P. Waghmare, Kaihong Zhou, Arjan Barendregt, Wiebke Westphal, Albert J. R. Heck, Egbert J. Boekema, Mark J. Dickman, and Jennifer A. Doudna. Rna-guided complex from a bacterial immune system enhances target recognition through seed sequence interactions. *Proceedings of the National Academy of Sciences*, 108(25):10092–10097, 2011.

[ZHA+13] Yan Zhang, Nadja Heidrich, Biju Joseph Ampattu, Carl W. Gunderson, H. Steven Seifert, Christoph Schoen, Jörg Vogel, and Erik J. Sontheimer. Processing-independent crispr rnas limit natural transformation in neisseria meningitidis. *Molecular Cell*, 50(4):488–503, 2013.

HPLC Standards

Table 1: Preparation of HPLC standards.

Compound	Molar Mass [g/mol]	Target [mM]	Mass [g]	Vol. [mL]	Actual [mM]
Sodium formate	68.01	100	0.1395	20	102.6
Sodium formate	68.01	75	0.1038	20	76.3
Sodium formate	68.01	50	0.0660	20	48.5
Sodium formate	68.01	25	0.0448	25	26.3
Sodium formate	68.01	200	0.3502	25	205.7
Sodium formate	68.01	150	0.2685	25	157.6
Sodium formate	68.01	100	0.1870	25	109.9
Sodium formate	68.01	75	0.1050	20	77.2
Potassium formate	84.12	200	0.4312	25	205.3
Potassium formate	84.12	150	0.3399	25	161.8
Potassium formate	84.12	100	0.2142	25	102.0
Potassium formate	84.12	75	0.1300	20	77.2
Methanol	32.04	100	0.0641	20	100.0
Methanol	32.04	50	0.0321	20	50.0
Isopropanol (70%)	60.10	50	0.0675	25	44.8
Sodium acetate	82.03	100	0.1641	20	100.0
Propanal	59.10	1500	0.7566	10	1302
Propanal	59.10	1000	1.1600	20	998.0
Propanal	59.10	1000	1.1560	20	995.0
Propanal	59.10	50	0.0581	20	50.0

Appendix B: Primer

Table 2: Verwendete Primer für die PCR

Primer Name	Target Region	Sequence
KWO_128	LHA-fw	AAATTGATGACGATTAAGTATCATAATTGCAACGCCAAA
KWO_129	LHA-rv	AAATTTTGGCGTTGCAATTATGATACTTAATCGTCATCA
KWO_130	pta-fw	GTATCGGGTCTCCAATTTGCTTATTTGATTTACATTATATAATATTG
KWO_131	pta-rv	CTCGATGGTCTCCCATGTTCATTTCCTCCCTTTAAATTTAAC
KWO_132	RS-fw	GTATCGGGTCTCC132
KWO_133	RS-rv	CTCGATGGTCTCCCATGTTGTTTCCTCCTAGTTG
KWO_134	RHA-fw	GTATCGGGTCTCCCATGCGATTTTTTCAAGTGAAAC
KWO_135	RHA-rv	CTCGATGGTCTCCAGCTCTCAATATCTGGCTGATCAC